Journal of Aerosol Science xxx (xxxx) xxx–xxx

Contents lists available at ScienceDirect

Journal of Aerosol Science

journal homepage: www.elsevier.com/locate/jaerosci

Review on the physics of electrospray: From electrokinetics to the operating conditions of single and coaxial Taylor cone-jets, and AC electrospray

Alfonso M. Gañán-Calvo[a,*], José M. López-Herrera[a], Miguel A. Herrada[a], Antonio Ramos[b], José M. Montanero[c]

[a] ETSI, Depart. Ingeniería Aeroespacial y Mecánica de Fluidos, Universidad de Sevilla, E-41092 Sevilla, Spain
[b] Depart. Electrónica y Electromagnetismo, Universidad de Sevilla, E-41012 Sevilla, Spain
[c] Depart. Ingeniería Mecánica, Energética y de los Materiales and Instituto de Computación Científica Avanzada, Universidad de Extremadura, E-06006 Badajoz, Spain

ARTICLE INFO

Keywords:
Electrohydrodynamics
Electrospray
Electrokinetics
Capillary jetting
Dripping

ABSTRACT

In this work, we review the physics of the liquid ejection by the application of electric fields, paying special attention to the steady cone-jet mode of electrospray. We aim to provide a comprehensive view on the role of electrohydrodynamics effects, and how the full electrokinetic equations can be reduced or simplified into the Taylor-Melcher leaky dielectric model. We provide an extensive review of the steady Taylor cone-jet mode, considering both its predicting scaling laws and limits of operation. Coaxial Taylor cone-jets are also briefly reviewed. Finally, we outline a revision of AC electrohydrodynamics and electrospraying.

1. Introduction

Many applications involving liquid handling at microscales take advantage of the inherently clean action of electromagnetic fields. Free ions are normally present in most molecularly simple liquid solvents. Assuming the most usual case where magnetic effects are negligible, only electric fields act on those ions. Electrokinetic phenomena are frequently referred to as the electric effects occurring at interfaces between immiscible phases. These interfaces form barriers preventing the continuous diffusion of free ions under applied electric fields. This provokes the accumulation of charges onto those surfaces. This effect and the jump of electrical permittivity in that region create strong local modifications of the surface forces and their equilibria. On the other side, electrohydrodynamics is the study of the evolution of electrically charged fluids owing to the action of both the surface forces mentioned above and the volumetric ones, caused by a non-zero space charge density and/or an electric permittivity gradient.

The richness of electrohydrodynamic phenomena encountered in microfluidics and capillary flows is fostered by the smallness of both the length and time scales, together with the usual presence of both convective and diffusive effects at comparable strengths. A careful identification of dominant and subdominant effects in a given system is paramount to achieve a correct modeling and eventual predictive tools to guide engineering designs. Current literature shows the fertility of this field, yet harboring some questionable hypotheses and results from simplifying models.

There is a large variety of phenomena caused by the action of intense electric forces on capillary systems. These phenomena include transient, periodic, quasi-steady and steady flows resulting from the competition between the electric driving forces and the

* Corresponding author.
E-mail address: amgc@us.es (A.M. Gañán-Calvo).

https://doi.org/10.1016/j.jaerosci.2018.05.002

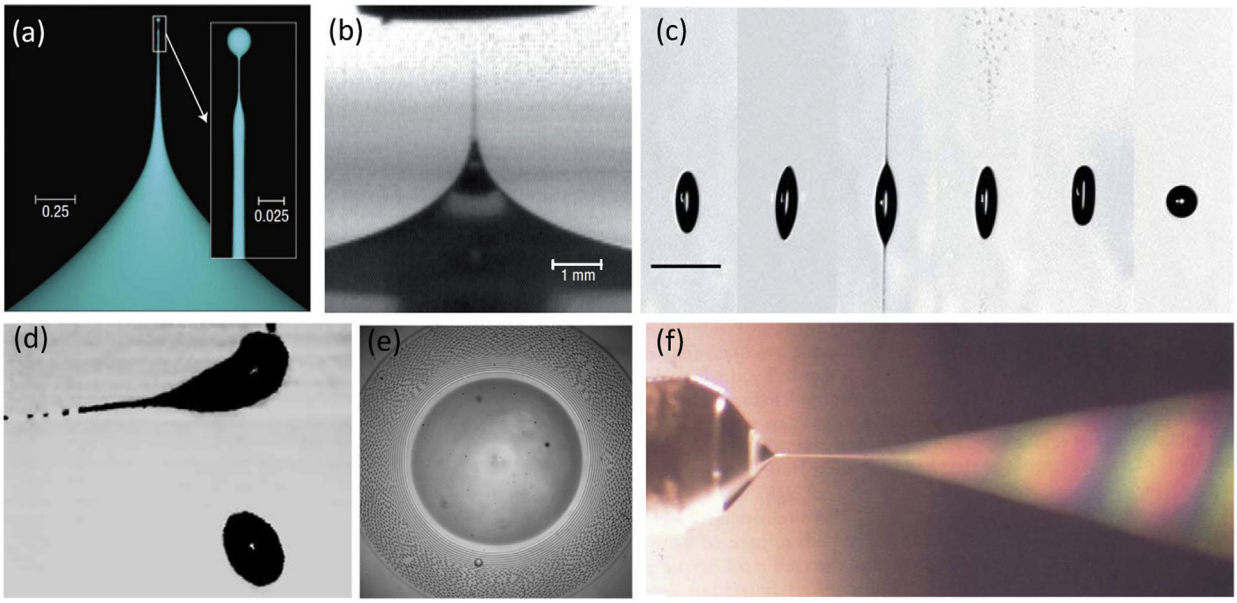

Fig. 1. Unsteady and steady modes of ejection from electrified capillary shapes. (a), (b) An electrified planar liquid interface develops a cusp-like instability ejecting an unsteady microjet over a threshold electrification level (Collins et al., 2008). (c) A levitated droplet is subject to an intense electric field that elongates it along the applied electric field direction, and provokes a double symmetric emission in opposite directions (Duft et al., 2003). (d) Micro-droplets ejected from a steady Taylor cone-jet overcome the Rayleigh limit by evaporation, become unstable, and undergo fission by ejecting a smaller scale microjet (Gomez & Tang, 1994). (e) A viscous liquid drop in another immiscible liquid bath is flattened by an applied electric field; under the right conditions, the drop eventually develops an equatorial rim-like instability that ejects a Saturn-like cloud of droplets (Brosseau & Vlahowska, 2017). (f) A classical steady Taylor cone-jet ejecting a spray of nearly monodisperse droplets. Observe the Tyndall effect producing a rainbow-like color distribution along the spray when it is properly illuminated (Pantano, Gañán-Calvo, & Barrero, 1994).

hydrodynamic ones, naturally arising when the liquid sets in motion. A general overview of ES processes is provided in Fig. 1. Planar charged interfaces may undergo cusp-like EHD emissions (Fig. 1.a and b, see Collins, Jones, Harris, & Basaran, 2008) when the charge level overcomes certain threshold, like in the case of charged droplets above the Rayleigh limit (Fig. 1.c and d), see Duft, Achtzehn, Müller, Huber, and Leisner (2003), Gomez and Tang (1994). Droplets in liquid environment subject to intense electric fields can also develop ejections perpendicular to the applied electric field for certain range of viscosities and permittivities ratios, leading to Saturn-like emission (Fig. 1.e) (Brosseau & Vlahowska, 2017). In the controlled EHD emission from an electrified capillary, the classical steady Taylor cone-jet and the resulting monodisperse spray is illustrated in (Fig. 1.f). Moreover, when an alternating AC electric field is applied, the variety of ejection phenomena depending on the characteristic times of the applied field compared to those of the system is enormous; here, the technological interest is focused on those which yield a controlled emission (e.g. pulsed drop-on-demand DoD, and AC electrospray). One of the salient characteristics of high frequency AC electrospray is the one-step ejection of lower charge or neutral droplets, which provides additional charge-mass characteristics (e.g. for mass spectrometry) and sometimes simplifies the experimental and production arrangements (e.g. biomaterials synthesis).

The complexity of electrohydrodynamics is difficult to find in other fields of mesoscale physics. Even in simple situations, where the system adopts a steady or quasi-steady regime, the high dimension of the parameter space and the lack of precise experimental information have precluded a comprehensive and accurate description of the problem. The steady Taylor cone-jet mode of electrospraying constitutes a very good example of this.

For the formation of a Taylor Cone-jet the liquid is polarized by applying a high voltage (HV) potential (hereafter referred as the *applied field*) to the liquid (applied directly to the liquid feeding capillary or needle, or to a immersed electrode) respect to a grounded electrode (usually a plate or a ring) located downstream. This leads to a intense electric field around the liquid drop pending or flowing from the capillary tube, deforming it into a cone-like shape from whose vertex the jet is ejected. A steady state is reached when the flow rate feeding the conical meniscus through the capillary needle equals the one released through the jet. The steady Taylor cone-jets naturally occurs under relatively limited circumstances: when the applied field and flow rate are in the appropriate range and the electrosprayed liquid exhibits the adequate physical properties, which entails having a field profile along the liquid surface necessary to get a potential drop in the liquid, from the polarizing electrode (either an immersed one, or the conductive capillary itself) to the cone apex, to accelerate the converging interfacial liquid to form the jet. This phenomenon exhibits certain physical balances and delicate symmetries which have attracted the attention of many investigators over the last decades, but even now fundamental questions about the mechanisms responsible for both the establishment of steady Taylor cone-jets and their stability remain unanswered. It is especially relevant to understand the origin of the instability taking place when the injected flow rate becomes smaller than a certain critical value, because this barrier limits the applicability of electrospraying in fields like analytical chemistry, with increasingly demanding standards of sensitivity, discrimination, etc.

In this paper, we review the fundamentals of electrospraying, focusing our attention on theoretical aspects of different phenomena arising when electric fields are applied onto simple and compound drops. At some points, steady cone-jet electrospraying will be compared to the flow focusing technique (Gañán-Calvo, 1998) (sometimes referred to as axisymmetric flow focusing) because of their similarities (Gañán-Calvo & Montanero, 2009): in both cases, an interface is subject to the action of focused forces. While those forces have an electrohydrodynamic origin in the former, they are purely mechanical in the later, i.e. produced by the converging stream of a focusing fluid (in many cases a gas) forced to flow through an orifice. We start in Section 2 by introducing the general models for electrokinetics, explaining how those models are coupled to the hydrodynamic equations to describe the transport of electric charges in a flowing medium. In Section 3, we derive the Taylor-Melcher leaky dielectric model, and justify its success to study the evolution of capillary systems with sizes much larger than the Debye layer thickness, and on time scales much longer than the electric relaxation time. We devote Section 4 to the steady Taylor-cone jet mode, deriving and discussing the scaling laws for the droplet size and current intensity. The specific characteristics of coaxial Taylor-cone jets are considered in this section too. As mentioned above, one of the fundamental aspects of the steady Taylor-cone jets that require further investigation is its stability. For this reason, this aspect of the problem is studied separately in Section 5, considering the limits of minimum and maximum flow rates as well as results obtained from the global stability analysis (resulting from the inspection of the growth rate of the spectrum of linear perturbation eigenmodes exhibited by the steady base flow). The linear stability of jets under different electric conditions is examined in Section 6. The paper closes with a brief revision on AC electrohydrodynamics and electrospraying in Section 7.

2. General models for electrokinetics

The structure and dissociation properties of molecular constituents of any liquid composition determine its electrokinetic behavior in two fundamental aspects for electrohydrodynamics and electrospraying applications in particular: (i) its electrical permittivity, and (ii) its electrical conductivity. The polarity of a molecule is determined by its electronic density distribution and its size (see Fig. 2): the larger the ratio of the distance between the centers of mass and charge densities to the molecular size, and the smaller this size, the larger the molecular polarity and consequently the electrical permittivity of the liquid. Besides, the molecular dissociation result and its equilibrium constant determines the mobility and concentration of ions of a liquid constituent, and therefore the electrical conductivity of the liquid, as subsequently illustrated.

Besides, given the high surface-to-volume ratio characterizing the manipulation of fluids at the microscale and its applications, physicochemical processes associated to interfaces are commonplace in those systems. The vast majority of them are operated at temperatures well below the critical point of the fluids involved and, therefore, solid, liquid and gas or vapor phases (if present) form completely separated domains. Thus, any physically consistent model for these systems should consider the conservation of mass, charge, momentum and energy, together with the equations of state, for each fluid constituent of the system. These elements must be used in combination with adequate models for the specific electrokinetic processes taking place at interfaces. Schematically, the macroscopic polarization of an electrolytic solution droplet under electric field $\mathbf{E}$ is illustrated in Fig. 3: the free charges (ions) of each polarity are displaced along the field lines $\mathbf{E}$ in opposite directions.

Assuming that no phase change occurs in a liquid phase, decoupling the conservation of mass, charge and momentum from the conservation of energy is a generally valid simplification. On the contrary, mass and energy conservation involving the liquid-vapor interface should be included in the model if evaporation is considered. The liquid can be manipulated by stress gradients of mechanical and/or electric origins, and by shear stresses introduced from interfaces (see Fig. 3.b) and resulting from the electric Maxwell stress and the mechanical tensors τ_e and τ_m, respectively:

$$\tau_e = \epsilon(\mathbf{EE} - |\mathbf{E}|^2\mathbf{I}) \quad \text{and} \quad \tau_m = -p\mathbf{I} + \tau_v = -p\mathbf{I} + 2\mu\gamma_{\mathrm{D}} \tag{1}$$

where ϵ is the electric permittivity of the fluid phase, $\mathbf{I}$ is the unit tensor, τ_v is the viscous stress tensor, p is the pressure, $\boldsymbol{\gamma}_{\mathbf{D}}$ is the gradient deformation tensor and μ is the viscosity of the fluid. The largest stresses are usually located at the interfaces where the

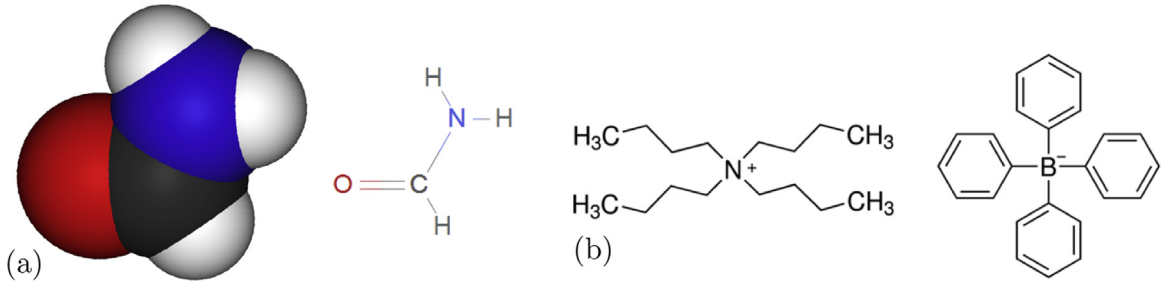

Fig. 2. (a) Example of highly polar liquid: formamide. Spatial, symbolic and graphic representations of its molecule. Its smallness and strong asymmetry of charge density yields extreme permittivity values ($\beta = 111$ at room temperatures). Dissociation: $NH_3CO \leftrightarrows CO^- + NH_3^+$. See also the video https://www.youtube.com/watch?v=g8WG17aMKzQ. The mobility of these ions provide large electric conductivities ($K > 10^{-2}$ S/m). (b) Molecular representation of an extreme example: a "ionic" liquid (Tetrabutylammonium tetraphenylborate), where the two large ionic constituents are shown. The large size and spatial symmetry of these molecules limit the polarity of the liquid ($\beta = 8.91$), while its conductivity remains relatively large compared to organic solvents ($K > 10^{-4}$ S/m).

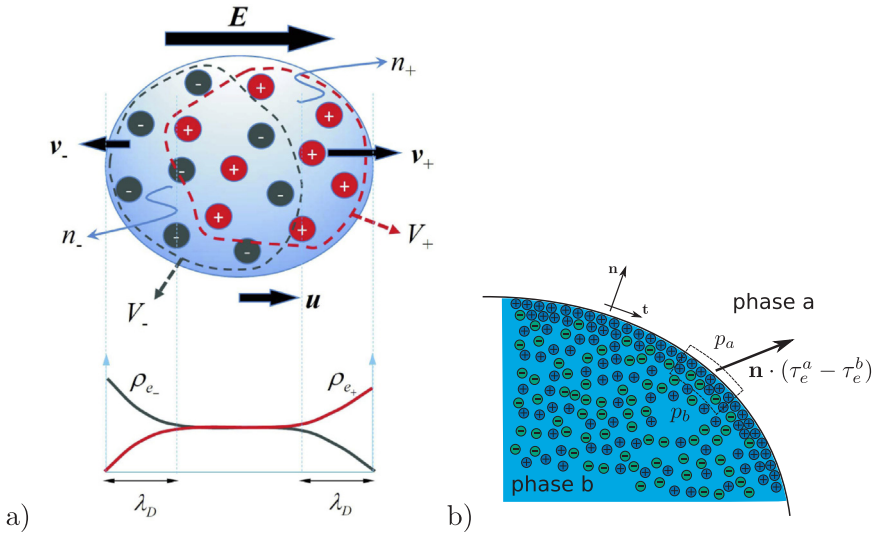

Fig. 3. (a) A droplet with two ionic species under the action of an applied electric field **E**. Here, v_+ and v_- indicate the local average velocities of species (+) and (-), respectively, while V_+ and V_- represent the volumes occupied by the species (+) and (-), respectively. (b) Sketch of stresses at a charged liquid interface separating phase a from phase b.

abrupt change in fluid properties occurs,

$$(p_b - p_a)\mathbf{n} + \mathbf{n}\cdot(\tau_e^a - \tau_e^b) + \mathbf{n}\cdot(\tau_v^a - \tau_v^b) = (\sigma\nabla\cdot\mathbf{n})\mathbf{n} + \nabla_s\sigma\mathbf{t} \tag{2}$$

where σ is the surface tension $\bigtriangledown_s$, stands for the surface gradient, and a and b are the fluid phases at either side of the interface.

The system dealt with in this work is always set in motion by the action of electrical and mechanical forces on the fluid constituents. As mentioned above, how these constituents behave under the action of those forces should be formulated as conservation equations, or adequate equivalent models (e.g., ion mobility), for each constituent. This entails a detailed knowledge of their electrochemical and electrokinetic features at every point of the domain, and in particular at interfaces.

The general formulation of any conservation principle reduces to an equation in integral form, which is particularly useful for numerical purposes, like in the Volume of Fluid (VoF) method. The conservation equation of the ionic k-species in integral form reads:

$$\frac{\mathrm{d}}{\mathrm{d}t}\int_{V_k} n_k \,\mathrm{d}V = \int_{V_k} \frac{\partial n_k}{\partial t}\mathrm{d}V + \int_{S_k} n_k\, \mathbf{v}_k\cdot\mathbf{n}\,\mathrm{d}A = \int_{V_k} r_k \mathrm{d}V, \tag{3}$$

where n_k is the number of mols per unit volume of the ionic k-species, V_k is the volume occupied by that species and surrounded by the closed surface S_k, $\mathbf{n}$ is the usual outer unit normal vector on S_k, r_k is the rate of production (mols per unit volume and unit time) by reaction, and $\mathbf{v}_k$ is the velocity of that species. This velocity can be expressed as the sum of three components: the average velocity of the fluid $\mathbf{u}$, the electric drift under the applied electric field $\mathbf{v}_{e,k}$, and the thermal diffusion velocity $\mathbf{v}_{d,k}$; i.e.,

$$\mathbf{v}_k = \mathbf{u} + \mathbf{v}_{e,k} + \mathbf{v}_{d,k}. \tag{4}$$

Both $\mathbf{v}_{e,k}$ and $\mathbf{v}_{d,k}$ can be expressed in terms of the local electric field and ionic concentration as:

$$\mathbf{v}_{e,k} = w_k e z_k \mathbf{E}, \tag{5}$$

$$\mathbf{v}_{d,k} = D_k \nabla \ln(n_k) = D_k \frac{\nabla n_k}{n_k}, \tag{6}$$

where w_k is the mobility of the k-species, z_k its valence, and e the elementary charge. These two migration mechanisms are not entirely independent since the diffusivity is related to the mobility of ions by the Einstein-Smoluchowski relationship, $D_k = w_k k_B T$, being k_B the Boltzmann constant and T the temperature.

The combination of the above Eqs. (3)–(6) results in the Nernst-Planck differential equation for the concentration of ionic species,

$$\frac{\mathrm{d}n_k}{\mathrm{d}t} = -\nabla\cdot[(w_k e z_k n_k\, \mathbf{E}) + D_k \nabla n_k] + r_k. \tag{7}$$

Also, a differential equation for the macroscopic charge density can be derived from Eq. (7):

$$\frac{\mathrm{d}\rho_e}{\mathrm{d}t} = -\nabla\cdot(K\,\mathbf{E}) + \sum_k D_k \nabla^2 \rho_{e,k} + \sum_k \xi_k, \tag{8}$$

where $\rho_{e,k} = N_A e z_k n_k = F z_k n_k$ and $\rho_e = \sum_k \rho_{e,k}$ are the ionic densities of the k-species and the net free charge density (charge per unit

volume), respectively. As usual, N_A and F are Avogadro's and Faraday's constants, respectively. Besides, $\xi_k = Fz_k r_k$ is the charge production rate of the k-species. The classical Nernst-Einstein approach allows a closed expression for the local value of the electrical conductivity of the liquid as

$$K = \sum_k w_k F\, e\, z_k^2 n_k\ . \tag{9}$$

For completeness, Maxwell equations (with the usual notations) provide the closing of the mathematical model:

$$\left.\begin{array}{l} \nabla\cdot\mathbf{D} = \rho_e \\ \mathbf{D} = \varepsilon_o\mathbf{E} + \mathbf{P} \\ \mathbf{P} = (\varepsilon - \varepsilon_o)\mathbf{E} \end{array}\right\} \Longrightarrow \nabla\cdot(\beta\mathbf{E}) = \frac{\rho_e}{\varepsilon_o}, \tag{10}$$

where ε_o and ε are the electrical permittivities of vacuum and the liquid (at the local conditions), respectively, and $\beta = \varepsilon/\varepsilon_o$.

In Eq. (8), two fundamental balances provide the most important spatial and temporal scales of all electrohydrodynamic problems with interfaces: the comparison between (i) thermal diffusion and electric drift, and (ii) temporal variations and electric drift. The first balance leads to the classical Debye's length λ_D appearing at interfaces, i.e., where molecular diffusion is halted by electric drift (see Fig. 3). In its most simplified form, λ_D can be obtained as:

$$\left.\begin{array}{l} \nabla\cdot(K\mathbf{E}) \sim \dfrac{K\rho_e}{\beta\varepsilon_o} \\ \sum_k D_k\nabla^2\rho_{e,k} \sim \dfrac{D_d\Delta\rho_e}{\lambda_D^2} \end{array}\right\} \quad \text{If} \quad \Delta\rho_e \sim \rho_e \Longrightarrow \lambda_D = \left(\frac{\beta\varepsilon_o D_d}{K}\right)^{1/2}, \tag{11}$$

where D_d can be taken as the diffusivity of the ionic species whose valence coincides with the polarity of the potential at the interface. On the other hand, the second balance mentioned above leads to the definition of the well-known electrical relaxation time t_e:

$$\frac{\mathrm{d}\rho_e}{dt} \sim \nabla\cdot(K\mathbf{E}) \Longrightarrow t_e = \frac{\beta\varepsilon_o}{K}. \tag{12}$$

When the electrokinetic model is considered, the dynamical evolution of an incompressible fluid can be calculated from the integration over the entire fluid domain (including the Debye layer) of the mass and momentum conservation equations,

$$\nabla\cdot\mathbf{u} = 0, \quad \rho\frac{\mathrm{d}\mathbf{u}}{\mathrm{d}t} = -\nabla p^* + \nabla\cdot\tau_\nu + \mathbf{f}_E, \tag{13}$$

where ρ, p*, and $\mathbf{f}_E$ are the liquid density, reduced pressure, p + ρ gz (g is the gravity and z the vertical coordinate) and electrical body force, respectively. The electrical body force $\mathbf{f}_E$ for an incompressible fluid is (Stratton, 1941)

$$\mathbf{f}_E = \nabla\cdot\tau_e = \rho_e\mathbf{E} - \frac{1}{2}E^2\nabla\varepsilon + \frac{1}{2}\nabla\left(E^2\frac{\partial\varepsilon}{\partial\rho}\rho\right), \tag{14}$$

where ε is the electric permittivity. In many cases, the numerical solution of the problem formulated above becomes computationally unaffordable due to the disparity between the Debye's length λ_D and the system size. Typical problems that require this calculation are those driven by AC fields (Chetwani et al., 2010; Chetwani, Maheshwari, & Chang, 2008a; Maheshwari & Chang, 2009; Yeo, 2005), the initiation of ejections from charged liquid surfaces (Gañán-Calvo, López-Herrera, Rebollo-Muñoz, & Montanero, 2016; Gomez & Tang, 1994; Pillai et al., 2016), naturally oscillating menisci with periodic emissions of charged liquid drops (Hijano, Loscertales, Ibáñez, & Higuera, 2015; Jaworek & Krupa, 1999), or the breakup of charged liquid jets (López-Herrera, Gañán-Calvo, Popinet, & Herrada, 2015). As will be explained in the next section, the Taylor-Melcher leaky dielectric model allows one to overcome this obstacle.

3. The Taylor-Melcher leaky dielectric model

As stated by Schnitzer and Yariv (2015), Bazant (2015), electrokinetics and electrohydrodynamic studies have proceeded in parallel turning their backs on each other. Electrohydrodynamic studies received their definitive impulse with the work of Taylor about the deformation of poorly conducting droplets in poorly conducting baths (Melcher & Taylor 1969). More recently, Schnitzer and Yariv (2015) culminated the work of Baygents and Saville (1989) to overcome the breach between these two disciplines. Using the problem of the droplet deformation, they rigorously derived the leaky dielectric model of Taylor and Melcher from an electrokinetic model by taking proper simplifications and limits. They showed that the leaky dielectric model can be justified as a macroscale version of the electrokinetic one if

- the droplet radius a is much larger than the Debye length λ_D; i.e., $\delta = \lambda_D/a \ll 1$
- the applied electric field is much larger than the electric field across the droplet caused by the thermal voltage; i.e., $\alpha = E/(V_T/a) \gg 1$, where a is the characteristic size of the domain, $V_T = k_B T/e$ is the thermal voltage ($V_T \approx 25$ mV at room temperature), and e the elementary charge.
- the applied electric field is much smaller than that associated with the thermal voltage in the Debye layer; i.e., $E \ll V_T/\lambda_D$ ($\delta\alpha \ll 1$).

The geometrical requisite $\delta \ll 1$ is needed to justify the interfacial nature of the leaky dielectric model. The condition $\alpha \gg 1$ implies that the diffusion current is much smaller than the conduction current (isotope diffusion, and anisotope field driven conduction). This and the uniformity of the ionic concentrations far away from the interface allow one to assume the bulk as an ohmic medium of constant conductivity. Electrohydrodynamic phenomena are characterized by intense applied fields amply verifying the condition $\alpha \gg 1$, while in electrokinetic problems α hardly reaches values of order unity. Since $\delta\alpha \ll 1$, the equilibrium in the Debye layers is slightly perturbed by the applied electric field, which allows the ohmic conduction through that layer. This requisite sets a limit in the strength of the applied electric field in order to preserve the structure of the Debye layer.

When the electric field applied to a capillary system forces the ionic species to displace according to their polarity, they eventually find an interface. This boundary halts the drift of ions in the direction of the applied field, which makes those ions accumulate near the interface in distances from the boundary of the order of λ_D. The phenomenon of charge accumulation at the interface takes place on times scales comparable to the electrical relaxation time. As mentioned above, this time is much smaller than the characteristic hydrodynamic time of the system and, therefore, the net charge in the bulk of the fluid domain becomes quasi-neutral almost instantaneously. This approximation can be formally expressed by the bulk equations

$$\frac{\rho_e}{\varepsilon} = \nabla\cdot\mathbf{E}_i = \nabla\cdot\mathbf{E}_o = \xi_k = 0. \tag{15}$$

The net charge accumulated near an element of the interface can be quantified by the surface charge density (charge per unit area) $\rho_{es} = \int_0^\infty \rho_e(z)dz$, where z is the coordinate normal to that interface element. If the structure of the Debye layer is not significantly altered by the applied electric field, the thickness of the layer next to the interface where $\rho_e \neq 0$ is of the order of λ_D. Consider a thin element of fluid at the interface. The area of the faces parallel to the interface is δA, while the thickness perpendicular to that surface is $\delta\ell$. Assuming that $\delta A^{1/2} \gg \delta\ell \gg \lambda_D$, Eq. (3) can be reduced to the conservation equation for the surface charge density

$$\frac{\mathrm{d}\rho_{es}}{\mathrm{d}t} = -\left\| K\mathbf{E} + \sum_k D_k \nabla\rho_{e,k} \right\|\cdot\mathbf{n} + \rho_{es}\mathbf{n}\cdot(\mathbf{n}\cdot\nabla)\mathbf{u}, \tag{16}$$

where $\mathbf{E}$, $\nabla\rho_{e,k}$ and $\mathbf{u}$ are evaluated at the interface, and $\|\|$ denotes difference between the outside and inside values. Saville (1997) provided a detailed alternative derivation of an equation equivalent to (16), which has served as a basic tool for most milestone works in this field since then. However, one should keep in mind that the use of the surface charge density is just a simplification to avoid high-spatial resolution numerical calculations near the interface. If those calculations are conducted, Eq. (16) is redundant, and one imposes the boundary conditions between two dielectric regions at the very surface which separates those regions.

The Taylor-Melcher leaky dielectric model (Melcher & Taylor, 1969; Saville, 1997) has become one of the most successful approaches to circumvent the complexity and computational cost of electrokinetics. This success has been such that it has been massively adopted without restrictions, sometimes outside its strict limits of applicability. An example of this is the analysis of highly unsteady electrohydrodynamic phenomena (Collins et al., 2008; Collins, Sambath, Harris, & Basaran, 2013), where electrokinetic effects should be carefully considered (Gañán-Calvo et al. 2016; Pillai et al., 2016). As mentioned above, Eq. (16) is a simplification which avoids the detailed spatial resolution of Eq. (8) for the space charge density $\rho_e(\mathbf{r}, t)$ in layers near interfaces with thicknesses of the order of λ_D.

As explained above, the application of electric fields to liquids with mobile ionic species in solution immediately leads to highly charged interfaces. Electrostatic forces practically vanish in the bulk, while strong electric surface forces arise near interfaces under those applied electric fields. These forces are calculated from the so-called Maxwell stresses evaluated at the interface:

$$\tau_n = \frac{\varepsilon_o}{2}[(E_n^o)^2 - (E_n^i)^2] + \varepsilon_o\frac{\beta-1}{2}[(E_t)^2 - (E_n^i)^2], \quad \tau_t = \rho_{es}E_t, \tag{17}$$

where ε_o is the vacuum permittivity, the subindexes n and t stand for the components normal and tangential to the interface, respectively, while the superindexes i and o denote that the quantity is evaluated on the inner and outer side of that surface, respectively. The leaky dielectric model is typically solved by finding the values of the electric potential in the inner and outer domains. For that purpose, the electric boundary conditions

$$E_t^i = E_t^o = E_t, \quad \rho_{es} = \varepsilon_o(E_n^o - \beta E_n^i) \tag{18}$$

are also considered at the interface.

In applying the leaky dielectric model, the conductivity is typically low enough for the tangential electric field to take significant values at the interface. This electric field, in combination with the surface charge, originates shear stresses on that surface, which may beget recirculation cells and other flow patterns under certain conditions studied in detail for example by Barrero, Gañán-Calvo, Dávila, Palacio, and Gómez-González (1998), Herrada et al. (2012). More interestingly, Maxwell stresses in highly charged interfaces induce vigorous motions, which can cause the breakup of those surfaces and liquid ejections, either steady or unsteady. The conditions under which the ejections can be steady are discussed in general terms in Sections 4 and 5.3. These steady ejections are the main object of the rest of this work due to their technological relevance for the continuous electrospray (ES) production of microdroplets with tunable charges and sizes. These droplets can yield tailored engineering particles or be applied to ES deposition for surface coating in various domains of applications (present issue shows many examples of materials, bio and energy related applications).

In summary, for the physicist interested in real applications where reproducibility and robustness of the system is a priority, steady systems are preferred. That is the case of the Taylor cone-jet configuration (Taylor, 1964; Zeleny, 1914, 1917), where Eq. (16)

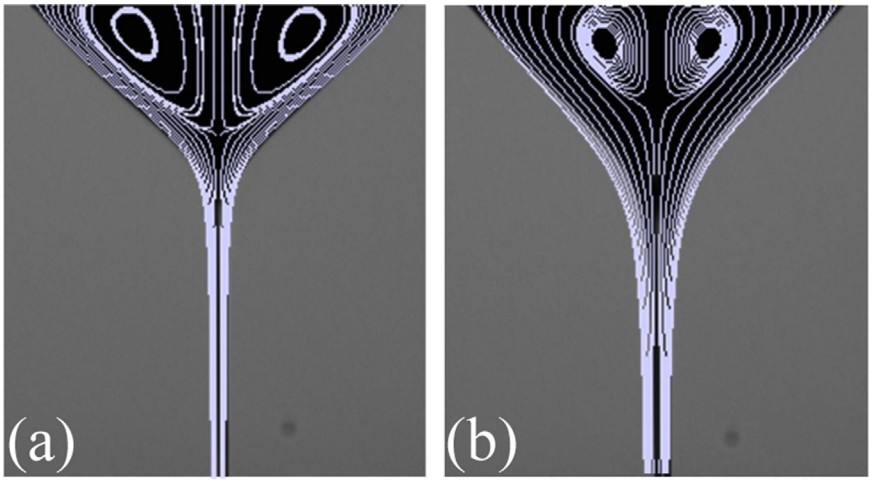

Fig. 4. Streamlines plotted on the corresponding experimental images for a 1-octanol cone-jet produced with $V = 1600$ V, and $Q = 0.5$ ml/h (a) and $Q = 1$ ml/h (b) (Herrada et al., 2012).

reduces to its steady form. The leaky dielectric model may even result superfluous for simple geometries like quasi-cylindrical jets, where a one-dimensional integral formulation of the conservation of momentum can be used (López-Herrera, Herrada, Montanero, Rebollo-Muñoz, & Gañán-Calvo, 2013).

4. The steady cone-jet mode of electrospray

In the steady cone-jet mode of electrospray, a meniscus hanging on a feeding capillary adopts a stable quasi-conical shape from whose apex a stationary thin jet is ejected. The jet eventually breaks up into droplets due to the capillary forces, which gives rise to a charged mist. All theories describing the physics behind the cone-jet mode distinguish three regions (Fernández de la Mora, 2007; Gañán-Calvo, 1997): (i) the upstream meniscus region attached to the capillary, where ohmic conduction is the dominant mechanism of charge transport and the voltage drop is negligible; (ii) the downstream jet region, where the relevant charge transport mechanism is surface convection; and (iii) an intermediate transition region (the cone neck), where the charge transport mechanism evolves from conduction-dominant to convection-dominant. It is generally accepted that both the electric current circulating through the system and the jet's diameter are essentially governed by this neck region. In addition, the charge relaxation time is much smaller than the residence time in the liquid meniscus, and thus variations of the space charge density in that region (coming, for instance, from the transfer of charge at the metal electrode-liquid interface) are quasi-instantaneously relaxed. Therefore, the charges are accumulated at the interface, and the leaky dielectric model constitutes the adequate theoretical framework to describe this problem. Fig. 4 illustrates this capability of this model.

4.1. Scaling laws

The most useful tools for electrospraying practitioners are the scaling laws predicting the order of magnitude of the size and charge of the emitted droplets. Given that the problem does not exhibit *complete similarity* (see Barenblatt, 2003, pages 82–91), dimensional arguments alone do not furnish those laws, and additional assumptions are required. Consider the cone-jet transition region of characteristic length L (Fig. 5) and defined as that where conduction and surface charge convection commensurate with each other. The cone tapers into a jet of radius R and velocity $v \sim QR^{-2}$ within this transition region, where the tangential electric field $E_t \sim (\sigma/\varepsilon_o L)^{1/2}$ is essentially determined by the Taylor cone. The scale of the electric current intensity is $I \sim KR^2E_t \sim KR^2[\sigma/(\varepsilon_o L)]^{1/2}$, while the power decay along the cone-jet transition region scales as $W \sim I\Delta\Phi \sim IE_tL \sim R^2\,K\sigma/\varepsilon_o$, where $\Delta\Phi$ is the voltage decay in that region. The energy budget of the system demands W to be of the same order of the kinetic energy flux $\rho v^2(R^2 v)$, and thus

$$R^2\frac{K\sigma}{\varepsilon_o} \sim \rho\frac{Q^3}{R^6}R^2 \Longrightarrow R \sim R_G = \left(\frac{\rho\varepsilon_o Q^3}{\sigma K}\right)^{1/6}, \tag{19}$$

where R_G is defined as the scaling proposed by Gañán-Calvo, Lasheras, Dávila, and Barrero (1994), Gañán-Calvo (1997), Gañán-Calvo (2004), Gañán-Calvo and Montanero (2009).

The above scaling was massively compared by Gañán-Calvo and Montanero (2009) with experimental measurements of emitted droplet diameter d, which commensurates with the jet size. We provide an illustrative graph showing this comparison in Fig. 6 (see Gañán-Calvo & Montanero, 2009 and the original publications cited therein for more details). In this figure, the flow rate Q and diameter d are made dimensionless with $Q_o = \sigma\varepsilon_o/(\rho K)$ and $d_o = [\sigma\varepsilon_o^2/(\rho K^2)]^{1/3}$, respectively. The scaling $d \sim R_G$ agrees with the experiments throughout the whole range of flow rates considered, even close to the minimum ones. The fitting yields a prefactor

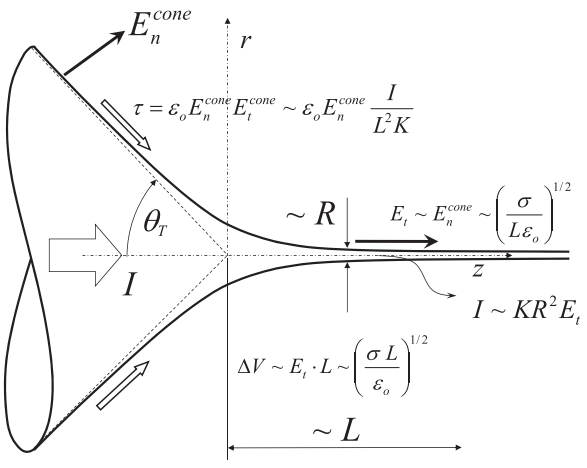

Fig. 5. Sketch of the steady Taylor cone-jet configuration showing the variables used for the calculation of the characteristic jet size and electric intensity. E_n^{cone} and E_n^{cone} stands for the normal and tangential fields on the surface of the conical meniscus region with characteristic length L.

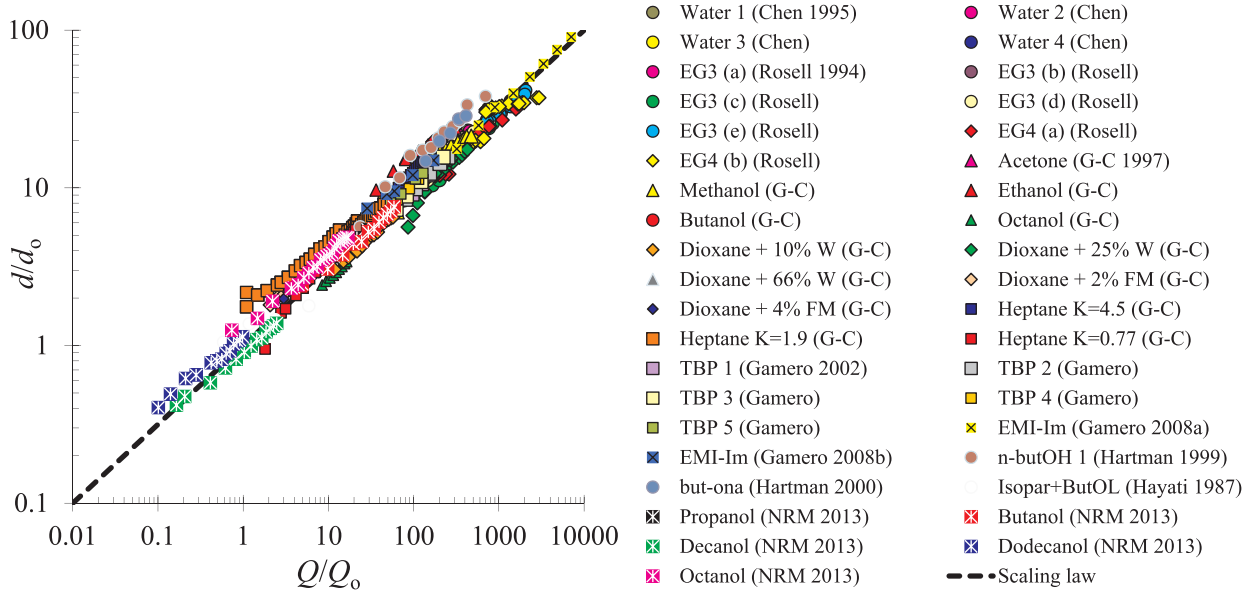

Fig. 6. Droplet diameter d measured by Chen, Pui, and Kaufman (1995), Rosell-Llompart (1994), Gañán-Calvo, Dávila, and Barrero (1997), Gamero-Castaño and Hruby (2002), Gamero-Castaño (2008a), Gamero-Castaño (2008b), Hartman, Brunner, Camelot, Marijnissen, and Scarlett (1999), Hartman, Brunner, Camelot, Marijnissen, and Scarlett (2000), Hayati, Bailey, & Tadros (1987a), and Rebollo-Muñoz (2013). See Ref. Gañán-Calvo and Montanero (2009) for more details. The dashed line is $d = R_G$.

approximately equal to one, and thus one can calculate with sufficient accuracy the emitted droplet diameter as

$$d = d_o(Q/Q_o)^{1/2}. \tag{20}$$

The electric charge transported by the jet can be determined in terms of the surface charge density in the cone-jet transition region (Gañán-Calvo, 1999). Assuming that inertia $\rho(QR^{-2})^2$ scales as the electrostatic suction $\varepsilon_o(E_n^o)^2$,

$$\varepsilon_o(E_n^o)^2 \sim \rho(QR_G^{-2})^2 \Longrightarrow E_n^o \sim \left(\frac{\sigma}{\varepsilon_o d_o}\right)^{1/2} \equiv E_o. \tag{21}$$

This means that the scaling of the surface charge density $\rho_{es} \sim \varepsilon_o E_o$ should be a universal value independent of the operating conditions (flow rate, applied voltage and geometry) (Gañán-Calvo, 1999). Then, the scale of the electric current transported by the jet moving at a speed $v \sim QR_G^2$ is

$$I \sim \varepsilon_o E_o (QR_G^{-2}) R_G \Longrightarrow I \sim (\sigma K Q)^{1/2} = I_o(Q/Q_o)^{1/2} \equiv I_G. \tag{22}$$

The scaling I_G was first derived and published by Gañán-Calvo, Barrero, and Pantano (1993). After some attempts trying to

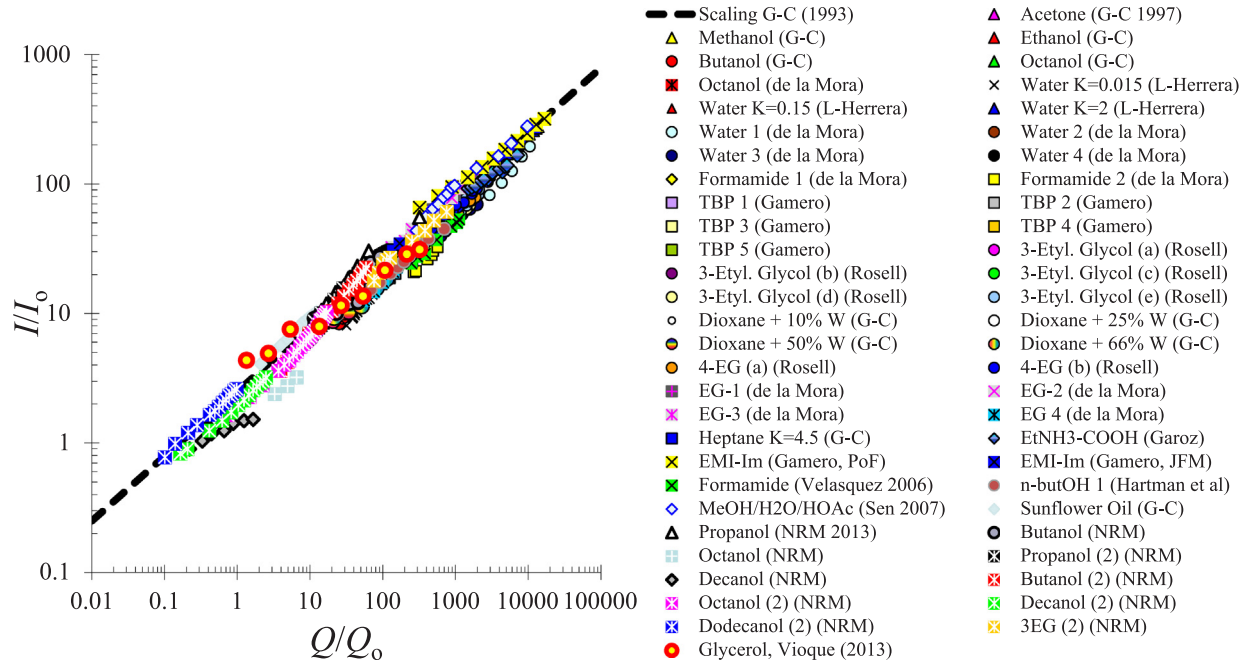

Fig. 7. Electric current intensity I measured by Fernandez de la Mora and Loscertales (1994), Gañán-Calvo et al. (1997), López-Herrera, Boucard, Loscertales, and Márquez (2004), Rosell-Llompart (1994), Gamero-Castaño and Hruby (2002), Gamero PoF (Gamero-Castaño, 2008a), Gamero JFM (Gamero-Castaño, 2008b), Garoz et al. (2007), Hartman, Brunner, et al. (1999), Velásquez-García, Akinwande, and Martínez-Sánchez (2006), Rebollo-Muñoz (2013), and Vioque-Martínez (2012). The dash line is $I = 2.5 I_G$.

reconcile discrepancies with experimental measurements that were difficult to attribute to the exponents of the scaling law (Gañán-Calvo et al., 1997; Gañán-Calvo, 1997), I_G was definitely endorsed by Gañán-Calvo (1999), Hartman, Brunner, et al. (1999), Gañán-Calvo (2004). Fig. 7 shows the comparison between I_G and about 2000 experimental measurements, which yields the fitting

$$I/I_o = 2.6(Q/Q_o)^{1/2}. \tag{23}$$

This validation supports the scaling hypotheses (Gañán-Calvo & Montanero, 2009; Gañán-Calvo et al., 1993; Gañán-Calvo, 1997, 1999, 2004), including the surface charge relaxation in the cone-jet transition region. This hypothesis is implicilty made when evaluating the electrostatic suction.

Finally, the scale of the transition region length L is given by the balance between the convective and conductive charge transports:

$$K\sigma(\varepsilon_o L)^{-1}R_G^2 \sim \varepsilon_o E_n^o Q R_G^{-1} \Longrightarrow L \sim d_o(Q/Q_o) \tag{24}$$

and, therefore, $L/R_G \sim (Q/Q_o)^{1/2}$. Because $Q/Q_o \gg 1$ in most realizations, the transition region is slender, and $E_n^o \gg E_t$ in that region.

Fernandez de la Mora and Loscertales (1994) derived other scaling laws for the jet radius and electric current intensity assuming the halt of surface charge relaxation in a region of the cone apex with size R_F of the order of the jet radius. This implies that the residence time of the liquid $t_r \sim R_F^3/Q$ in that region should be comparable to the charge relaxation time $t_e = K/\varepsilon$ (Fernandez de la Mora & Loscertales, 1994). This immediately yields $R_F = (\beta\varepsilon_o Q/K)^{1/3}$ independently of any stability consideration. The scale $I_F \sim \nu R_F \varepsilon_o E_n^o \sim (\sigma K Q/\beta)^{1/2}$ of the electric current was easily obtained from R_F, since $\nu \sim Q/R_F^2$ and $E_n^o \sim (\sigma/(\varepsilon_o R_F))^{1/2}$ (the latter expression is derived from the capillary-electric stress balance in the jet). The prediction for the jet's size matched the experimental data reported by Fernandez de la Mora and Loscertales (1994) reasonably well within the experimental errors in the measurements. However, a matching of similar quality for the electric current intensity required an ad hoc adjustment of the role played by the liquid permittivity in the scaling law: $I \simeq f(\beta) I_F$, with $f(\beta)$ spanning over an order of magnitude.

The timely introduction of these scalings and their success has earned Fernández de la Mora a deserved predominance and authority in the field. In fact, nearly all research works on electrospray physics to date start from these scalings without caveats; many of them (see, e.g., Cherney, 1999; Higuera, 2017) share the same foundational hypothesis that the jet size and electric current are determined by the limit of surface charge relaxation without restrictions or criticism. However, the comparisons in Figs. 6 and 7 irrefutably show that the scalings R_G and I_G globally fit their corresponding experimental data far better that any alternative model so far, an indication that the hypotheses leading to R_G and I_G reflect the general physics of actual steady Taylor cone-jets more accurately. As mentioned above, in contrast with other models, these hypotheses include (since Gañán-Calvo et al., 1993) the surface charge relaxation in the cone-jet transition region, whose size L is much larger than the jet's radius.

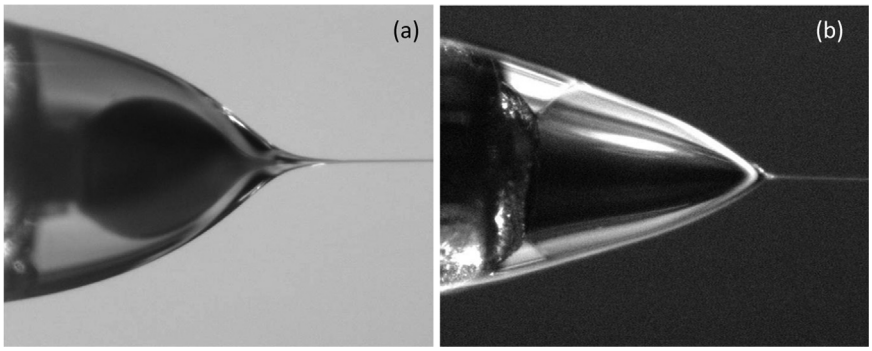

Fig. 8. (a) Coaxial Taylor cone-jet with an outer driver. The outer and inner liquids are Somos additive ($K = 6.25 \times 10^{-5}$ S/m, $\mu = 7.5 \times 10^{-1}$ Pa · s) and colored ethylene glycol ($K \simeq 10^{-5}$ S/m, $\mu = 1.6 \times 10^{-2}$ Pa · s), respectively. (b) Coaxial Taylor cone-jet with an inner driver. The outer and inner liquids are olive oil ($K < 10^{-8}$ S/m, $\mu \simeq 7 \times 10^{-2}$ Pa · s) and ethylene glycol ($K \simeq 1.1 \times 10^{-5}$ S/m, $\mu = 1.6 \times 10^{-2}$ Pa · s), respectively. Cortijo and Loscertales 2000, private communication.

4.2. Coaxial Taylor cone-jets

Micrometer coaxial jets were produced for the first time in 1998 (Gañán-Calvo, 1998) with the flow focusing technique. Subsequently, the same idea was applied to produce coaxial electrified jets (Loscertales et al., 2002) on the basis of the analogies between flow focused (mechanical) and Taylor (electrical) cone-jets. The impact of that result was extraordinary, and there has been an enormous development along this line since then. Coaxial Taylor cone-jets have been fundamentally applied to the generation of complex fibers (Greiner, 2007; Li & Xia, 2004), and, to a lesser extent, to the production of complex particles (Ahmad et al., 2008; Chen, Zhao, Song, & Jiang, 2008; Choi et al., 2010; Huang et al., 2006; Marín, Loscertales, Márquez, & Barrero, 2007; Park & Braun, 2010; Valo et al., 2009; Xie, Marijnissen, & Wang, 2006; Xie, Ng, Lee, & Wang, 2008; Xu & Hanna, 2006; Yang, Lu, Xiang, & Luo, 2007; Zhao & Jiang, 2009). The different working modes of this configuration were described by Chen, Jia, Yin, Cheng, and Lu (2005), relating them to those appearing in the single-component electrospray. The steady regime and the initiation phase were analyzed by López-Herrera et al., 2003 and Reznik et al., 2006, respectively. The driving liquid is the one with the largest electrical conductivity. In the most common configuration, that role is played by the external liquid phase in contact with the outer environment (whether a vacuum, gas or dielectric liquid) (Chen, Jia, et al., 2005) (see Fig. 8a), although the inner liquid acted as the driver fluid in the original configuration (see Fig. 8b) (Loscertales et al., 2002).

The differences between the coaxial electrospray driven by the external liquid and the corresponding single-phase case are minimal, except when the flow rate of the inner liquid becomes comparable to or larger than that of the outer one, in which case the stability of the system is affected. The outer driver shields the inner liquid from the applied electric field, and the whole two-phase bulk becomes nearly equipotential. When the viscosity of the outer driver relative to that of the inner liquid is not too large or small, the diameter of the compound jet is similar to that of the single-phase electrospray for the same flow rate as that of the driver. In this case, the inner liquid acts nearly as a hollow core from the mass continuity standpoint, since the electrohydrodynamic velocity is fixed by the driver.

When the flow is driven by the inner liquid, the latter tends to reach the meniscus free surface, expanding the interface exposed to the applied electric field (see Fig. 8b). In this case, one expects the flow rate of the outer liquid to be small as compared to that of the driver. This occurs as long as the viscosity of the outer liquid is not large as compared to that of the driver. On the contrary, if the viscosity of the outer liquid is sufficiently large, momentum is efficiently transferred to the external liquid bulk, and the outer flow rate can be large in terms of that of the driver (see Fig. 6B in López-Herrera et al., 2003). In addition, the possible injection of charge from the driver into the outer liquid extends the stability of the system (Larriba & Fernandez de la Mora, 2011).

5. Stability of the steady cone-jet mode of electrospray

5.1. Equilibrium shapes of electrified menisci. Role of applied electric potential and boundary conditions

In the process of formation of a steady cone-jet configuration after a liquid spout is ejected, since the issuing spot modifies the volume of the parent meniscus, a first fundamental question arises: what would be the range of liquid restitution rates to sustain a steady emission of liquid in the form of a steady microjet?

The answer to this question entails two main considerations:

1. Stability:
   (a) Underlying electrohydrostatic solutions may act as possible attractors of the dissipative dynamical system. In one hand, non-emitting stable hydrostatic menisci with rounded apex and fixed volume exist for a wide range of applied voltages. On the other hand, an infinite Taylor cone is a theoretical universal static solution which, properly adapted to finite applied EF + BC (see Pantano et al., 1994) furnish theoretical electrohydrostatic (non emitting) solutions with pointed apexes. These solutions

exist for a specific value of the applied electric voltage Φ_o, a given volume of the meniscus V_o, a given geometry of the tube where the meniscus is attached (fundamentally determined by its diameter D), and given set of boundary conditions (e.g., the tube-electrode distance H for a flat electrode perpendicular to the tube) (Pantano et al., 1994). See also the introduction of Higuera (2017) and references therein for a concise summary on non-emitting electrified menisci.

(b) Minimum flow rate: why pointed-apex solutions complying with EF + BC that would sustain an asymptotic regime with vanishing liquid emission *are not attained* in reality? In this regard, are the interesting solutions of *infinitesimally thin jets* of Cherney (1999) attainable (i.e., *stable*)?

2. Space charge effects:
   (a) The charged issuing jet modifies the electric field distribution of the parent meniscus (Gañán-Calvo, 1997). Maximum flow rate: is there a maximum size of the jet for which a cone-jet would be globally unsustainable?
   (b) Depending on the relative length of the jet to the meniscus, the presence of the charged spray may affect the meniscus directly (Fernandez de la Mora, 1992) or indirectly, by affecting the value of the applied voltage needed to re-equilibrate the whole electric field distribution between the feeding tube and the electrode (Gañán-Calvo et al., 1994; Grifoll & Rosell-Llompart, 2012; Hartman et al., 1999). In the latter case, the influence of the spray demands a voltage increase that in general is a small fraction of the total applied voltage.
   (c) The strong electric fields on the liquid surface around the cone-jet transition region may provoke local ion evaporation and surrounding gas ionization (gas discharges). In the cases of large surface tension and liquid conductivities (e.g. water), experimental evidence suggests that no steady Taylor cone can operate in air at standard conditions without gas discharge (i.e., emitted charge that is not transported by the issuing droplets) (Borra et al., 1996; Borra, Tombette, & Ehouarn, 1999; Borra et al., 2006). The jet can even be stabilized by the presence of the ionized gas (Borra, Ehouarn, & Boulaud, 2004).

A first conclusion from prior discussion and the experimental evidence is that the applied voltage, meniscus volume and ejected liquid flow rate are three variables with an existing interdependency. A pedagogic approach to understand this interdependency is provided by electrohydrostatic solutions: if those could be attained in the limit of vanishingly small issued flow rates, one would asymptotically recover a genuine voltage-volume independency. This is addressed in the following. Subsequently, the limits of stability of steady cone-jets will be discussed in detail.

5.1.1. Theoretical electrohydrostatic solutions

Intuition suggests that a non-emitting solution underlies any steady Taylor-cone-jet based on the fact that the immense majority of the system volume is quasi-hydrostatic. In reality, the presence of the jet could be assumed as a small perturbation to the hydrostatic solution (Gañán-Calvo, 1997). However, even though the singularity of the apex makes it locally unstable, no one knows so far whether a hydrostatic solution where the apex would be artificially fixed (for example setting a microscopically or asymptotically small plug at the apex to prevent emission) could be globally stable: a subject of further studies. In spite of that physical conundrum, the basic relationship between the applied voltage and the volume (or elongation) of the meniscus of an electrohydrostatic solution in the absence of emission can be obtained. Moreover, general solutions of the classic perpendicular tube-flat plate configuration for variable H/D ratio can also be attained. Following the work of Pantano et al. (1994), one reaches to the following expression (a fitting with less than 0.2% error):

$$\gamma_1^* = \ln\left(\frac{4H}{D}\right)\left(1 + 0.00082\ln\left(\frac{4H}{D}\right)\right)(0.3 + 0.35\tau^{-1/2} + 0.075\tau^{-2}), \tag{25}$$

where γ_1^* is the critical value of the Taylor number $\gamma_1 = (\varepsilon_o\Phi_o^2)/(\sigma D)$ for which a meniscus with a conical apex is a hydrostatic solution, and τ is the given non dimensional volume of that meniscus ($\tau = Vo/R_o^3$, $R_o = D/2$). It should be noted that in expression (25) the liquid attaches to the inner edge of the tube, with radius $0.8R_o$ (see configuration in Pantano et al., 1994), and the edge has a 45° to approximately provide a continuation of the conical electrohydrostatic solution of the liquid meniscus. The limits of validity of this expression are for $0.25 < \tau < 1.2$, $10 < H/R_o < 100$ (probably $10 < H/R_o < 1000$). Here, the only relevant property of the liquid is its surface tension σ. There is a minimum applied voltage below which no equilibrium shape can be obtained. Besides, there is a turning point or minimum volume of the meniscus, which would correspond to the applied voltage above which the cone tilts laterally, and the axisymmetric electrohydrostatic solution would not be stable according to experimental observations.

Then, after the first issuing spout tapers, keeping the electric field constant drives the system towards different possible situations. The evolution takes place in characteristic times that depend on the size of the tube at which the meniscus is attached. If the tube continuously feeds a liquid flow rate comparable to the one that can be naturally extracted by the spout, the system can reach to a steady state: a steady Taylor cone-jet where the volume or the elongation of the meniscus in equilibrium depends on the applied voltage and the liquid flow rate. However, as discussed in Section 5.1, steady cone-jets cannot be stable for any arbitrary values of applied voltages or liquid flow rates. This is addressed in the following.

5.2. The limits of steady Taylor cone-jets

Historically, the expression “steady jetting” has been coined in the microfluidics literature to refer to the emission from a stationary liquid source of a jet that remains almost intact over a distance long compared to its diameter. Beyond that distance, the jet

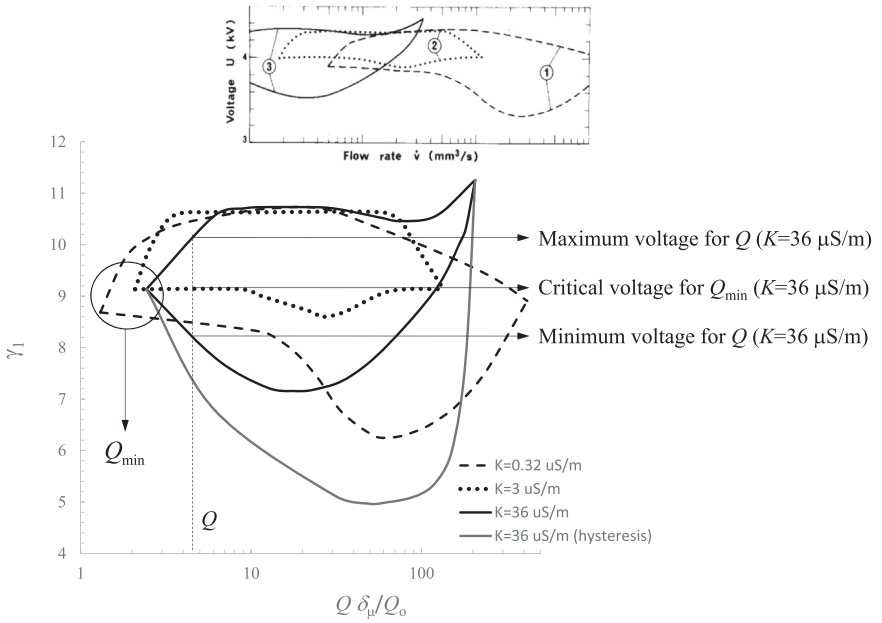

Fig. 9. Domains of existence (stability) of Taylor cone-jets for dioxane with small amount of formamide to attain different values of the electric conductivity, according to Cloupeau and Prunet-Foch (1989). The distance needle to plate was $H = 10$ mm and the inner radius of the feeding capillary tube was $R_o = 0.25$ mm. Here, $\gamma_1 = (\varepsilon_o \phi_o^2)/(2\sigma R_o)$, where ϕ_o is the applied voltage and R_o is the external radius of the feeding capillary tube (Pantano et al., 1994).

may either break up into droplets due to the Rayleigh capillary instability or oscillate laterally owing to the whipping instability (Eggers & Villermaux, 2008). The cone-jet mode of electrospray falls into the steady jetting category.

For a given applied voltage, geometry, and liquid properties, there is a specific range of flow rates -if any- for which that steady state or steady solution exists, bounded by a minimum and maximum flow rate values. Alternatively, for a given flow rate, there is a range of voltages for which a steady cone-jet is possible. The first quantitative description of such fundamental map of stability in the voltage-flow rate parametrical space for a given geometry and liquid properties was given by Cloupeau and Prunet-Foch (1989). Fig. 9 shows such maps for a given geometry ($H = 10$ mm, $D = 0.5$ mm; here, three different liquids are explored (dioxane with different small concentrations of formamide to change its conductivity) and the liquid attaches to the outer edge of the tube with diameter D.

Naturally, the ejected jet and spray produces a space charge whose immediate effect on the cone is a decrease of the electric field on the surface of the meniscus, and consequently an elongation of the equilibrium conical shape. The first analytical model to account for this effect assuming that (i) the issuing spray had a conical shape as well, and (ii) the jet was very small (i.e., the spray issued right from the apex of the meniscus) was proposed in Fernandez de la Mora (1992). Subsequently, an asymptotic analytical model including an issuing jet with slowly varying shape and its effect on the cone was proposed in Gañán-Calvo (1997), from which the analytical asymptotic shape of the jet and the scaling laws of the jet size and the issuing current were also obtained. In general, for a fixed value of the applied voltage, the larger the flow rate the more elongated the meniscus is.

Steady Taylor cone-jets reach to global stability limits owing to different causes. First, regarding the applied voltage, for a given flow rate there is a minimum voltage below which the elongation of the conical meniscus becomes unsustainable. By carefully adjusting that voltage, a very elongated meniscus that some authors have termed “silver bullet mode” can be observed (Chen et al., 1995; Szostek et al., 1997). This is consistent with the electrohydrostatic solutions according to Pantano et al. (1994). On the other hand, there is a maximum voltage above which the jet tilts laterally (Cloupeau & Prunet-Foch, 1994). In spite of this, a steady non-symmetric cone-jet solution would still exist. However, above certain voltage threshold, multiple jet emission develops (Cloupeau & Prunet-Foch, 1989, 1994; Hayati et al., 1987a; Jaworek & Krupa, 1999).

On the other hand, for an applied voltage inside the domain of stability of the cone-jet mode, there is a minimum and a maximum flow rates at which the system becomes unstable. The minimum and maximum flow rate instabilities have a completely different origin: while the former in general initiates at a region of the cone close to the cone-jet neck by a dynamical unbalance of kinematic, surface tension and electrical forces (normally, the electrical forces can no longer sustain the liquid “extraction” from the cone), the later normally initiates at the jet by an excess of charge (Cloupeau & Prunet-Foch, 1989). In the following, we discuss the mechanisms underlying such instabilities and describe them quantitatively in terms of general non-dimensional parameters.

5.3. Minimum flow rate

The diameter of the jet emitted in the cone-jet mode of electrospray decreases as the injected flow rate decreases and, therefore, so

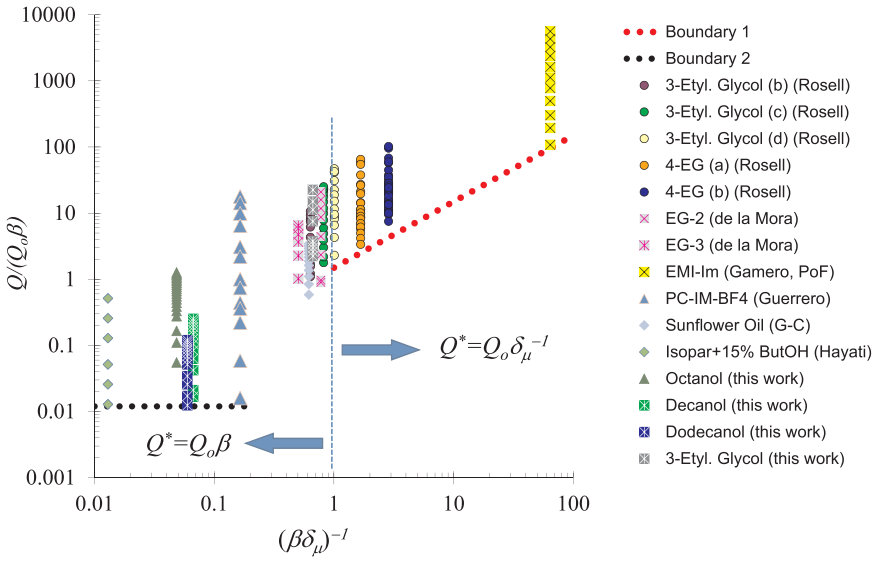

Fig. 10. Minimum flow rate in the steady cone-jet mode (Fig. 2 in Ref. Gañán-Calvo et al., 2013). The symbols correspond to experimental steady jetting realizations, while the dotted lines are the scaling laws $Q_{\min} = Q_o\beta$ and $Q_{\min} = Q_o\delta_\mu^{-1}$.

does the size of the droplets resulting from the jet capillary breakup (Gañán-Calvo & Montanero, 2009). Close to the minimum flow rate stability limit (see Fig. 9), a relatively monodisperse stream of droplets is produced with their minimum size. This confers considerable technological interest on this limit, which has been a subject of continuous debate for electrospray practitioners and researchers since the beginning of its systematic analysis (Chen et al., 1995; Cherney, 1999; Fernandez de la Mora & Loscertales, 1994; Fernández de la Mora, 2007; Gañán-Calvo et al., 1997; Gañán-Calvo, 1997, 1999, 2004; Gañán-Calvo, Rebollo-Muñoz, & Montanero, 2013; Hayati, Bailey, & Tadros, 1987b; Higuera, 2010, 2017; Rosell-Llompart & de la Mora, 1994; Scheideler & Chena, 2014; Smith, 1986; Smith, Alexander, & Stark, 2006). The fact that this limit is frequently bounded by a regular oscillating (dripping) regime, as occurs in aerodynamic flow focusing (Cruz-Mazo, Montanero, & Gañán-Calvo, 2016; Gañán-Calvo & Montanero, 2009), has attracted the attention of researchers as well (Chen, Saville, & Aksay, 2006; Hijano et al., 2015; Juraschek & Röllgen, 1998; Stark, Alexander, & Smith, 2014).

We define $Q_{\min}$ as the minimum flow rate attainable in the flow rate-applied voltage parameter plane (see Fig. 9). It means that there is a particular value of the voltage for which this flow rate is reached. In operating the electrospray with voltages above or below that value, one may have the impression of reaching $Q_{\min}$, but the flow rate to establish a stable cone-jet is simply an upper bound of $Q_{\min}$.

Dimensional analysis of the minimum flow rate limit has been tackled by several authors (Gañán-Calvo et al., 2013; Higuera, 2017; Scheideler & Chena, 2014). Gañán-Calvo et al. (2013) rationalized experimental results for the minimum flow rate in terms of the balance between the forces driving and opposing the liquid ejection in the cone-jet transition region (Fig. 10). If polarization forces raise against the ejection, the minimum flow rate $Q_{\min}$ scales as $Q_{\min} \sim Q_o\beta$ (Fernandez de la Mora & Loscertales, 1994; Gañán-Calvo et al., 1997; Higuera, 2017). If viscous forces stall the jet, $Q_{\min} \sim Q_o/\delta_\mu$. These two scenarios correspond to $(\beta\delta_\mu)^{-1} \ll 1$ and $(\beta\delta_\mu)^{-1} \gg 1$, respectively. In the region $\beta \sim \delta_\mu$ of the (β, δ_μ) parameter plane, the polarization and viscosity forces are comparable to each other, and the minimum flow rate $Q_{\min}/Q_o = f(\beta, \delta_\mu)$ is not expected to verify any of those scaling laws. It must be noted that these results rely on the local character of the jet emission. For very viscous liquids, the cone-jet transitional region spans a length scale comparable to the inner nozzle radius, R_o, and the minimum flow rate can be affected by that length (Scheideler & Chena, 2014). In addition, small conductivities may lead to jet diameters only one order of magnitude smaller than those of the nozzle, which does not ensure the locality of the jet emission.

For low-viscosity and relatively high-conductivity liquids, the scalings for $Q_{\min}$ proposed by Fernandez de la Mora and Loscertales (1994), Fernández de la Mora (2007) were formally justified by Gañán-Calvo et al. (2013), Higuera (2017). Higuera (2017) considered several alternative theoretical scenarios and scalings for the electrically induced flow rate Q_e in the low and high polarity and viscosity cases, suggesting that Q_e could be a proxy of $Q_{\min}$; a central question not addressed is the global stability of the corresponding theoretical limits proposed. Although no experimental verification was provided by Higuera (2017), some of the scaling laws for Q_e agree with those previously proposed and validated for $Q_{\min}$. Specifically, the flow rate $Q_e \sim \beta\sigma\varepsilon_o/(\rho K)$ calculated for high polarity and low viscosity agrees with the corresponding experimentally tested scaling of $Q_{\min}$ in Gañán-Calvo et al. (2013). In addition, the flow rate $Q_e \sim \sigma\varepsilon_o/(\rho K)$ obtained for low polarity and viscosity is the reference value Q_o assumed to be the minimum one in early studies (Gañán-Calvo et al., 1993; Gañán-Calvo, 1997, 1999).

The role of the capillary tube was considered in neither Gañán-Calvo et al., 2013 nor Higuera, 2017. Given the stabilizing effect of the triple contact line anchorage, the tube radius may also become an important parameter. Scheideler and Chena (2014) proposed the scaling $Q_{\min} \sim \sigma R_o^2/\mu$ for viscous liquids of limited conductivity. Interestingly, this coincides with the minimum flow rate of flow

focusing for sufficiently high viscosities (Montanero et al., 2011), probably because the two configurations share the same instability mechanism. For low viscosity liquids, the mechanism leading to $Q_{\min} \sim R_o\mu/\rho$ for flow focusing (Vega et al., 2010) may also apply to electrospray. In this case, the recirculation in the cone induced by the tangential surface stresses (Barrero et al., 1998) can be stalled at the inner surface of the tube, which induces the global instability of the system. Thus, in the parametrical region of low viscosity and relatively large conductivity liquids (e.g. water of aqueous solutions), using extremely small feeding capillary sources (i.e. R_o typically below 10 microns, sometimes below 100 nm -see Haywood et al., 2015) leads to what is known as nano-electrospray (e.g. Morelle & Michalski, 2007; Wilm et al., 1996). This procedure offers very robust and reproducible output (emission). Interestingly, it has been even used as a probe for local sample analysis (Saha-Shah et al., 2015), where the technique has been termed Scanning Electrospray Microscopy (Yuill, Shi, Poehlman, & Baker, 2015). The scaling laws for the emissions at those nano-scales are expected to follow those of the larger Taylor cone-jets counterparts, but this is still an area of open research.

5.4. Maximum flow rate

For a given applied voltage, a maximum flow rate is reached when the cone-jet develops an oscillating or unsteady regime associated with either the level of charge carried by the jet or the maximum flow rate that the jet can evacuate. As explained in Section 4.1, the total amount of charge is proportional to the square root of the flow rate ejected. The charge placed by the jet in front of the electrified cone diminishes the electric field on its surface, and increases the voltage needed to keep it at equilibrium. Sometimes, this voltage increase alters the charge transported by the jet, which may trigger unstable modes that grow in the jet and affect the cone (Cloupeau & Prunet-Foch, 1989, 1994). In other cases, one observes that the cone grows and eventually issues a liquid blob that continues emitting liquid (spindle mode), which shows the inability of the jet to evacuate the injected flow rate. In some experimental realizations, the jet charge level is such that the surrounding gas ionizes, and thus the net normal electric field on the jet surface decreases. This produces a stabilizing effect on the cone-jet, which significantly increases the maximum flow rate (Borra et al., 2004; Jaworek at al., 2014; Tang & Gomez, 1995). In this case, there can be polarity effects related to the different nature and mobility of the charge transporting ions (Kim et al., 2014; Pongrác et al., 2016). In any case, the charge emitted close to the maximum flow rate limit cannot be considered a small perturbation with respect to that located in the quasi-electrohydrostatic region. For this reason, the maximum flow rate limit involves a broad variety of complex issues, wider than that appearing in the minimum flow rate case.

5.5. Global stability analysis

A rigorous global stability analysis of the steady cone-jet configuration involves the calculation of the underlying base (unperturbed) flow, and the eigenfunctions of the linearized Navier-Stokes operator for that flow. If the spectrum of eigenvalues is in the stable complex half-plane, the base flow is linearly and *asymptotically* stable, which means that any initial small-amplitude perturbation will decay exponentially on time for $t \to \infty$ (as long as the linear approximation applies) (Theofilis, 2011). If the linearized Navier-Stokes operator is normal, then the perturbation energy decreases monotonously on time not only in the asymptotic regime but also during the system's short-term response and, therefore, linear *asymptotic* global stability implies linear stability (Schmid, 2007). Herrada et al. (2012) calculated numerically the base flow of the cone-jet mode from the leaky dielectric model. However, and to the best of our knowledge, the asymptotic global stability analysis of that base flow has not as yet been conducted. The recent development of a numerical technique for this purpose (Herrada & Montanero, 2016) opens the door to a rigorous study of the cone-jet mode stability even for moderately large conductivities (i.e. large R_o/d_o values) and small flow rates (i.e. Q close to Q_{min}), which give rise to a disparity between the size of the liquid meniscus and the emitted jet.

Fig. 11 shows the profiles of four cone-jets calculated for the corresponding minimum flow rates. Observe that the polarity β and the combined viscosity-polarity parameter $\beta\delta_\mu$ span around one order of magnitude. The voltage was adjusted in each case to obtain the best matching of the profiles in the cone-jet transition region. The radial and axial distances were made non-dimensional with the characteristic length $r_t = \beta^{1/6}R_G$ proposed by Gamero-Castaño (2010) (Fig. 11(a)), and with $R_T = R_o^{2/3}d_o^{1/3}$ (Fig. 11(b)). The profiles

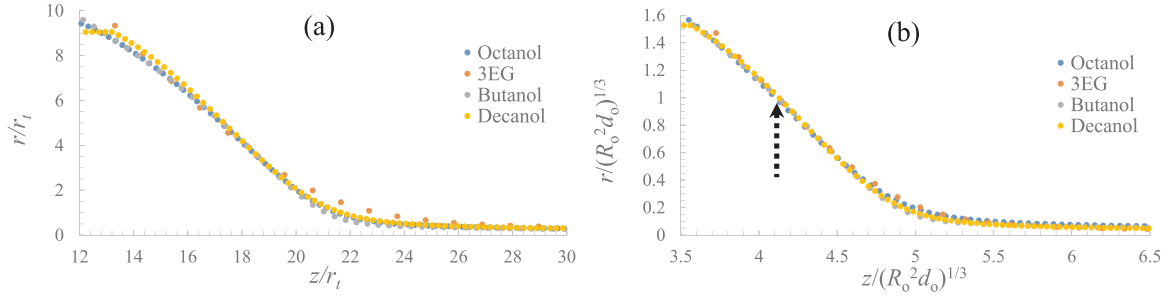

Fig. 11. Cone-jet profiles for a given set of liquids calculated at the corresponding minimum flow rates. (a): Profiles scaled with characteristic length r_t proposed by Gamero-Castaño (2010) (b): Profiles scaled with characteristic length $R_T = R_o^{2/3}d_o^{1/3}$. The arrow indicates the point at which the amplitude of the eigenmode responsible for instability reaches a maximum. The radius of the capillary R_o is located at different values of the ordinates according to the non-dimensional definitions.

collapse quite well using r_t, except at the center of the cone-jet transition. However, the best collapse is found using the scale R_T independently of the liquid polarity. The arrow in the figure indicates the point at which the amplitude of the eigenmode responsible for instability reaches a maximum. This point is approximately the same in all the cases when the profiles are scaled with R_T.

6. Jet instabilities and breakup

This section is aimed at those interested in the physics of the mechanisms behind the Taylor cone-jet decay into droplets (spray). In the absence of published global stability results (i.e., those from stability analyses involving the whole cone-jet domain), we are left with those derived from the *local* analysis applied to the emitted jet. Due to the relative simplicity of this analysis, studies have proliferated in this area, constituting a significant body of literature. In this section, we review some of the major results obtained about both the local linear stability and nonlinear breakup of a electrified jet due to their relevance for the steady cone-jet mode of electrospray. We restrict ourselves to liquids subject to DC electric fields and surrounded by hydrodynamically passive dielectric media because these are the conditions typically found in electrospray realizations. The studies reviewed in this section have considered perfectly and weakly conductors, with zero, small or large viscosities, both in the absence of a fixed applied electric field (the so-called charged jets) and subject to axial or radial uniform fields. Although the cone-jet mode of electrospray is more related to the weakly conductor and axial electric field case, we will review some results for the other configurations as well.

A fundamental starting point of the analysis is the assessment of the charge level in both the jet and the issuing droplets compared to the Rayleigh stability limits of perfectly conducting fluid masses (Rayleigh, 1881). In the case of a sphere of radius r_e, the limit charge is $q_{eR} = 8\pi(\varepsilon_o \sigma r_e^3)^{1/2}$. Besides, the limit charge of a cylinder of radius r and length l is $q_{cR} = \sqrt{6}\pi(\varepsilon_o \sigma r\, l^2)^{1/2}$. If the volume of the jet segment with slenderness $\lambda = l/r$ equals that of the droplet that it begets, then one has $r_e/r = (0.75\lambda)^{1/3}$. Then, the ratio of sphere (droplet) to cylinder (jet) Rayleigh limit charges would be:

$$\frac{q_{eR}}{q_{cR}} = \sqrt{8/\lambda} \tag{26}$$

Then, assuming conservation of charges at jet breakup and increasing the jet charge, for $\lambda > 8$ the droplet would reach the limit charge *before* the jet does. For an uncharged infinite capillary cylinder, Rayleigh predicted that the most probable breakup slenderness (wavelength) λ is given by the root of the equation:

$$\frac{d}{dx}\left(\frac{x\mathrm{I}_1(x)}{\mathrm{I}_0(x)}(1-x^2)\right) = 0, \tag{27}$$

where $x = 2\pi/\lambda$ is the perturbation wavelength of an axisymmetric breakup. It yields $\lambda = 9.01436... > 8$; in case that the same λ would apply to a charged jet, the droplets would undergo Rayleigh fission while the jet remains below the Rayleigh limit. This is often observed for a charged jet breakup (see Cloupeau & Prunet-Foch, 1989, Fig. 18a, and Gomez & Tang, 1994), back to the earliest observations reported in the literature (Zeleny, 1917). Thus, the determination of the most probable breakup mode and wavelength is paramount to determine the fate of the resulting charged droplets from electrospray.

6.1. Axisymmetric instability

In the local stability analysis, the perturbation wavelength is assumed to be much shorter than both the hydrodynamic and electric axial characteristic lengths and, therefore, the emitted jet could be seen as an infinite cylindrical liquid column either electrically charged or subject to an axially uniform electric field. The capillary time provides the time scale characterizing the temporal evolution of jets with small viscosity. For charge relaxation times much smaller than that characteristic time and limited electric conductivity, the leaky dielectric model applies. Under the action of an axial electric field, shear electric stresses at the interface bend the velocity profile in leaky dielectric jets, and surface charge is redistributed by both conduction and fast fluid reaction to variations in the tangential stress (Mestel, 1994). Although these effects considerably hinder the stability analysis of electrified jets, the simplicity of this configuration would still allow one to calculate analytically the dispersion relationship, which gives the mode eigenfrequency as a function of its wavenumber (Mestel, 1994).

The conclusions derived from the local stability analysis tell us little about the boundaries of the parameter region where the cone-jet mode of electrospray can be found. They rather allow us to understand the mechanisms leading to the jet break up or its lateral oscillation downstream. For instance, it is well known that the surface charge enhances the axisymmetric instability responsible for the breakup of a perfectly conductor inviscid jet, a result obtained by Taylor (1969) correcting a flawed equation of Basset (1894). Similarly, radial electric fields externally applied to perfectly conducting jets with coaxial electrodes also augment that instability (Collins, Harris, & Basaran, 2007; Hartman et al., 2000). Specifically, they increase the range of unstable wavenumbers, the growth factors, and the most unstable wavenumber (Collins et al., 2007; Hartman et al., 2000). These effects can be simply explained in terms of an increase of the effective surface tension owing to the electric stress normal to the interface. On the contrary, axial electric fields are known to stabilize conducting jets, reducing both the interval of unstable wavelengths and growth factors of varicose perturbations (Li, Yin, & Yin, 2006).

López-Herrera, Riesco-Chueca, and Gañán-Calvo (2005) examined the linear stability of a imperfectly conducting viscous jet subject to a radial electric field considering non-plug basic flows. They concluded that limited conductivity may significantly affect the jet stability. This study was extended to coflowing jets by Li, Yin, and Yin (2008). In this case, the radial electric field stabilizes/

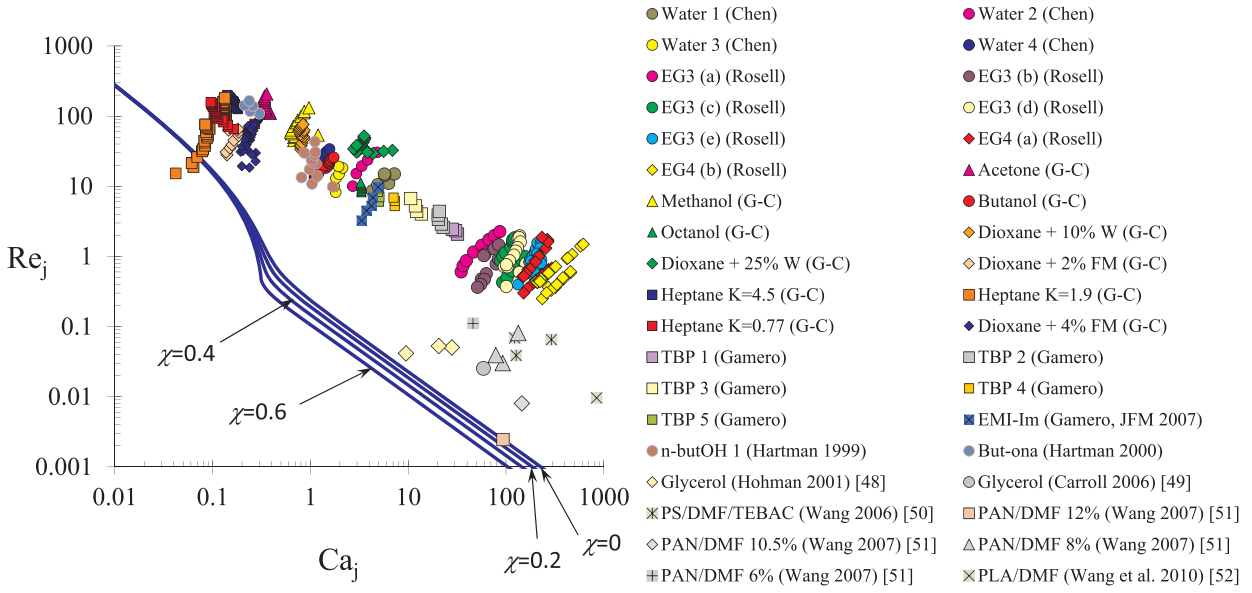

Fig. 12. Convective to absolute instability transition for an uniformly charged jet (Fig. 5 in - López-Herrera et al., 2010). The transition curves (solid lines) are calculated in terms of the Reynolds number $\mathrm{Re}_j = \rho v_j d_j/(2\mu)$, the capillary number $\mathrm{Ca}_j = \mu v_j/\sigma$ and the Taylor number $\chi = d_j \varepsilon_o E_o^2/(2\sigma)$. The symbols correspond to electrospray steady jetting realizations. The Taylor number affects the convective-to-absolute instability transition only for sufficiently large (small) values of the capillary (Reynolds) number (the Stokes limit).

destabilizes the jet for electrical Euler numbers (the ratio of normal electric stress to inertia) smaller/larger than a certain critical value (Li et al., 2008). Mestel (1994, 1996) calculated the growth factors of the varicose mode in a low-conductivity jet accelerated by an axial electric field for both low (Mestel, 1994) and high (Mestel, 1996) viscosities. In the low viscosity case, the shear at the free surface caused by the tangential electric stress suppresses the surface tension instability, but excites the electric one for large enough values of the velocity gradient (Mestel, 1994). In addition, all the axisymmetric temporal modes of a very viscous jet can be stabilized if both the surface charge and applied electrical field take suitable values.

6.2. *Convective-to-absolute instability transition*

The spatiotemporal stability analysis of the dispersion relationship for the axisymmetric mode enables one to determine the convective or absolute character of the jet's instability as a function of the Weber number (the ratio of the convective to capillary speed) (Leib & Goldstein, 1986). The concept of convective instability captures the behavior of a moving system that is stable at a fixed station but develops instabilities carried along (or *convected*) by the system, and is a requisite for steady jetting because otherwise growing capillary waves would travel upstream precluding the jet formation (Huerre & Monkewitz, 1990). In contrast, absolute instability reflects the system unstable character at a fixed station. Artana, Touchard, and Romat (1997) analyzed the convective-to-absolute instability transition in a perfectly conductor and inviscid jet flowing inside a coaxial cylindrical electrode. López-Herrera, Gañán-Calvo, and Herrada (2010) studied the appearance of absolute instability in uniformly charged, perfectly conductor, viscous jets. They found that the critical Weber numbers are hardly affected by the Taylor (electric Bond) number (the ratio of the normal electric stress to the capillary one) except in the Stokes limit, where absolute instability is enhanced by the surface charge (Fig. 12). Li, Gañán-Calvo, and López-Herrera (2011) showed that an axial electric field may hinder the convective-to-absolute instability transition of low permittivity and low conductivity jets. The comparison between the predictions of the spatiotemporal stability analysis and experiments (see Fig. 12) clearly indicates that the convective instability is a necessary but not sufficient condition for steady jetting stability. Indeed, the analysis sometimes predicts that the jet would be convectively unstable (i.e. locally stable) in cases where the cone-jet becomes unstable for much larger flow tares. In other words, there must be instabilities arising upstream from the jet and making the cone-jet unstable while the jet would be otherwise convectively unstable. This is the case specifically illustrated in Fig. 11, where the arrow indicates the point where the most unstable eigenmode exhibits its maximum amplitude: observe that this point is located significantly upstream of the jet.

To summarize, the stability analysis of electrified jets consistently shows that surface charge and externally applied radial electric fields destabilize the jet. This effect manifests itself by increasing both the critical Weber numbers leading to absolute instability and the growth rates of the varicose mode responsible for the jet breakup. The opposite occurs when axial electric fields are applied. The cone-jet mode of electrospray typically produces jets very long as compared to their diameters. This is possible due to the stabilizing effect not only of the axial electric field but also of the small Reynolds number characterizing these jets for large enough conductivities. In this case, the growth factors are much smaller than the inverse of the capillary time, and the dominant perturbation wavelength significantly increases (Tomotika, 1935).

6.3. Whipping instability

The jet emitted by a Taylor cone in a hydrodynamically passive dielectric medium may develop the so-called *whipping instability* (Eggers & Villermaux, 2008). This instability gives rise to non-axisymmetric (lateral) oscillations which cause the fast and violent lashes of the charged jet. Lord Rayleigh (1881) originally explained this phenomenon in terms of the decrease (increase) of electric (interfacial) energy caused by the lateral displacement of a perfectly conducting charged jet. His calculations led to the so-called *Rayleigh limit* for the superficial charge carried by a cylinder. The whipping instability in a perfectly conductor jet can also be explained as follows: if a small portion of the jet moves slightly off its axis, the charge re-distributes instantaneously along the surface in such a way that the electrical forces will push that portion farther away from the axis. This mechanism resembles what occurs in a high-speed jet moving in a quiescent gaseous bath or, conversely, in a jet coflowing with a high-speed gaseous stream. In both cases, the gas pressure forces play that destabilizing role. In any case, the bending of the jet causes very large tensile stresses, which lead to a violent jet thinning. This effect is beneficial in electrospinning because it enhances the solvent evaporation rate, and thus favors the fiber formation.

In principle, the whipping instability of an electrified jet can be either convective or absolute depending on whether the lateral oscillations are swept away by the stream or climb upstream reaching the liquid source. However, absolute whipping has not as yet been identified in electrospray/electrospinning experiments. Taylor (1969) conducted the temporal linear stability analysis of the $m = 1$ mode for a charged inviscid jet, and obtained the minimum charge per unit length for that mode to be unstable. Mestel (1994), Mestel (1996) calculated the growth factors of the lateral mode in a low-conductivity viscous jet accelerated by an axial electric field. Sinuous waves with logarithmically large wavelengths were found to be unstable. Li, Yin, and Yin (2009) considered the stability of a leaky dielectric shell enclosing dielectric core in a radial electric field. This field was found to have a strong destabilizing effect on nonaxisymmetric modes, especially those having smaller azimuthal wavenumbers.

Regarding the viscosity of the liquid, non-Newtonian effects are very relevant in the cone-jet mode of electrospray because they are at the root of the fiber formation in electrospinning. Since it is out of scope of this review on electrospray for the production of droplets suspended in gases, for aerosol processes, electrospinning for fiber formation without jet break-up is simply mentioned with references for models. In this technique, the polymers contained in the solution are stretched when crossing the cone-jet transition region. The polymer stretching increases the liquid extensional viscosity, which inhibits the varicose instability and enhances the jet whipping. As mentioned above, whipping causes a violent thinning of the emitted jet, which favors the solvent evaporation and therefore the fiber solidification. As in the Newtonian case, the global stability analysis of the cone-jet mode of electrospinning requires the calculation of the corresponding base flow from the leaky dielectric model. For this purpose, a nonlinear constitutive relationship must be adopted to replace Newton's law (Bird, Armstrong, & Hassager, 1987; Bird et al., 1987; Carroll & Joo, 2008; Clasen et al., 2006; James, 2009; Li & Yin, 2011; Li, Gañán-Calvo, López-Herrera, Yin, & Yin, 2013; Xie, Yang, Qin, & Fu, 2017; Yang, Liu, & Fu, 2012). Here, the simple Olroyd-B model has been frequently proposed to calculate the polymer stresses arising in ultra-dilute solutions. To the best of our knowledge, the base flow of the cone-jet mode of electrospinning has not as yet been calculated even for such a simple rheological model, and much less its linear stability. Besides, the Newtonian and slender-body approximations have also been considered to examine the stability of electrospun jets with small diameter variations (Shin, Hohman, Brenner, & Rutledge, 2001). The shape of the whipping envelope can be accurately calculated with a Lagrangian model, where the jet is discretized in terms of small segments subject to electrical forces (Reneker & Yarin, 2008).

6.4. Breakup

The growth of the linear axisymmetric mode cannot entirely explain the jet's breakup because of the nonlinear effects arising during the last phase of the process. The full hydrodynamic equations must be integrated over time to properly describe the free surface pinch-off. This calculation is time-consuming because all the forces diverge as the capillary system approaches that instant. To overcome this obstacle, one-dimensional models have been considered as in other similar problems (Eggers, 1993). These models essentially rely on the slender shape of the jet as well as on the fact that viscous diffusion of momentum ensures almost flat velocity profiles in that region. The one-dimensional approximation can be derived from the Navier-Stokes equations and exact boundary conditions by keeping only the leading-order terms in Taylor expansions in the radial coordinate of both the axial velocity and pressure, but retaining the exact free surface curvature and Maxwell stresses (Eggers & Dupont, 1994). Despite the fact that the jet adopts non-slender shapes before its breakup, the model provides accurate predictions for significant characteristics of that process, such as the size and charge of both the primary and satellite droplets formed after the breakage of a conducting jet subject to a radial electric field (Collins et al., 2007; López-Herrera & Gañán-Calvo, 2004). However, details of the breakup process like the existence/absence of free surface overturning in that zone cannot be captured by the one-dimensional approximation. Conroy, Matar, Craster, and Papageorgiou (2011) extended the nonlinear slender jet approximation to the case where ionic surfactants and electrokinetic effects are present. Numerical simulations of that model predict that electrostatic and electrokinetic effects increase the size of satellite droplet but have a rather weak influence on the breakup time. In addition, the ionic surfactants are swept away from the pinching region and, therefore, the system follows the self-similar dynamics of clean viscous jets at times close to the breakup time. This result is questionable because of both the limitations inherent to the one-dimensional approximation and the absence of surface viscous stresses which can substantially modify the transport of surfactants over the free surface (Ponce-Torres, Montanero, Herrada, Vega, & Vega, 2017).

Collins et al. (2007) solved the full Navier-Stokes equations to simulate the breakup of a cylindrical jet of a perfectly conductor liquid in a radial electric field when a periodic perturbation is triggered. They showed that nonlinear effects generally delay the jet

breakage, and the jet profiles at the incipience of pinch-off are considerably affected by the electric stresses. The one-dimensional model reproduced reasonably well the qualitative features of the jet profile provided that the electric Bond number does not take too large values. The size of the primary/satellite droplet decreases/increases as the electric Bond number increases. This effect becomes more noticeable as the Ohnesorge number increases. Wang (2012) solved the leaky dielectric model in the Stokes limit for a jet immersed in a liquid bath and a radial electric field. Finite conductivity significantly affects the breakup process and the pinch-off dynamics. López-Herrera et al. (2015) analyzed the breakup of a charged liquid column of low conductivity calculating the evolution of the volumetric charge density, and taking into account the resulting spatial dependence of the electric conductivity. Their results show that the distribution of electric charges between primary and satellite droplets considerably changes when the electrical conductivity is not constant for small enough Debye lengths.

7. AC electrohydrodynamics and electrospray

In this section, we consider procedures where the electrical actuation is varied in time following a sinusoidal input. Depending on the ratio of the characteristic time of the actuation to the one of the dynamical response of the electrified meniscus, one may distinguish two limiting regimes: drop-on-demand (DoD) or forced dripping, when that ratio is large (Chiarot, Gubarenko, Mrad, & Sullivan, 2009; Reznik et al., 2006; Reznik, Yarin, Theron, & Zussman, 2004; Tran, Byun, Nguyen, & Kang, 2009; Tran, Byun, Yudistira, & Oh, 2011), and AC electrospray (Chetwani et al., 2008b; N. Chetwani, C.A. Cassou, D.B. Go, & H.-C. Chang, 2010, 2011; Yeo et al., 2004; L.Y. Yeo, Gagnon, & Chang, 2005) (in contrast with the common DC electrospray) in the other limit. In between, for intermediate frequencies, AC electrospray from liquid hanging from a wire polarized at 50 Hz above a plane counter electrode (i.e. with a planar symmetry of the electrospray setup rather than the classical axisymmetric electrospray from a nozzle) is described by Borra et al. (1999), with two unipolar cones and spray produced successively at each half period on different sides of the wire.

DoD and dripping procedures usually result in highly controllable and repeatable droplet generation, with the drawback that the drop to meniscus size ratio is not small. In contrast, AC electrospray has been shown to yield small-scale ejections within the appropriate (sometimes restrictive) parametrical domain. In this review, we restrict ourselves to this latter case for its technological importance in biomaterials synthesis (Yeo et al., 2005) and mass spectrometry (Chetwani et al., 2010). Before that, for the interested reader we put into context the AC electrospray by deriving the equations describing AC electrohydrodynamic phenomena.

7.1. AC electrohydrodynamics

DC electric fields are widely employed in microsystems to control microparticles suspended in electrolytic solutions, particularly, by using electrophoresis and/or electroosmosis (Manz et al., 1992; Stone, Stroock, & Ajdari, 2004). Direct currents in electrolytes require that there are Faradaic (red-ox) reactions at the interface between the electrode and liquid: electrons must be transferred from metal electrodes to liquid molecules and vice versa. In general, electrodes must be placed outside the device to avoid generation of bubbles and/or electrochemically generated new species. AC electric fields generated by microelectrodes mounted inside microchannels can be used instead, with advantages such as lower power requirements, simple integration, and little or no electrolysis issues. In addition, electrical properties of particles and fluids vary with signal frequency, which opens new ways of actuation as, for example, the dielectrophoresis of particles (Pohl, 1978).

Fluid flows of electrolytic solutions subjected to AC voltages in microsystems can mainly appear from electrical forces in the liquid bulk (e.g., gradients of conductivity and permittivity actuated by electrothermal forces), or in the Debye layer near interfaces (e.g., the double layer between electrode and electrolyte actuated by AC electro-osmotic forces). In both cases, the applied electric field exerts force upon charge that is induced by the electric field itself. The electrical force is quadratic with the field amplitude and, therefore, it has a non-zero time-average for AC electric fields, leading to continuous fluid flow (Castellanos, Ramos, Gonzalez, Green, & Morgan, 2003).

7.1.1. Simplified equations

In the liquid bulk, the electrical current can be simplified in many situations to Ohm's law. In effect, diffusion current is typically much smaller than conduction current if the voltage drop across the bulk is much greater than the thermal voltage ($V_T = k_B T/e \approx 25$ mV at room temperature). For electrolytes, convection of charge is also negligible compared to conduction, as demonstrated by the small electrical Reynolds number $R_E = \varepsilon u/K\ell \ll 1$, where ℓ is the characteristic length of the variation of the electric field, potential, ion concentration, …(Castellanos et al., 2003). In this situation, the charge conservation equation becomes

$$0 = \nabla\cdot\mathbf{j} + \frac{\partial \rho_e}{\partial t} = \nabla\cdot\left(K\mathbf{E} + \varepsilon\frac{\partial \mathbf{E}}{\partial t}\right). \tag{28}$$

Assuming that the liquid conductivity and permittivity vary in times much longer than the period of the applied AC signal, the charge conservation equation can be written using phasors as

$$0 = \nabla\cdot(K\mathbf{E} + i\varepsilon\omega\mathbf{E}), \tag{29}$$

where ω is the frequency of the AC signal. This equation, together with the fact that the field is irrotational, determines $\mathbf{E}$. Poisson's equation is used to obtain the induced charge density:

$$\nabla\cdot(\varepsilon\mathbf{E}) = \rho_e. \tag{30}$$

In fact, Poisson's equation tells us that electrolytes are quasi-electroneutral in the bulk. In effect, for a ion monovalent solution,

$$\frac{n_+ - n_-}{n_+ + n_-} = \frac{\nabla\cdot(\varepsilon\mathbf{E})}{eN_A(n_+ + n_-)} \sim \frac{\varepsilon\mu_e E}{K\ell}, \tag{31}$$

where μ_e is the ion mobility multiplied by the elementary charge. For typical electric fields and lengths about one micron or greater, this ratio is much less than one. However, the small difference between the concentrations of positive and negative ions is sufficient to generate observable forces.

In order for the induced charge to be different from zero, there must be gradients in conductivity and/or permittivity. Using the charge conservation Eq. (29), the induced charge becomes

$$\rho_e = \nabla\cdot(\varepsilon\mathbf{E}) = \frac{\mathbf{E}\cdot(K\nabla\varepsilon - \varepsilon\nabla K)}{K + i\varepsilon\omega}. \tag{32}$$

The electrical body force for an incompressible liquid can be written as (Stratton, 1941)

$$\mathbf{f}_E = \rho_e\mathbf{E} - \frac{1}{2}E^2\nabla\varepsilon, \tag{33}$$

where the electrostriction term has been omitted and incorporated into a redefined pressure. The time-averaged electrical body force is then (Ramos, Morgan, Green, & Castellanos, 1998)

$$\langle\mathbf{f}_E\rangle = \frac{1}{2}\mathrm{Re}\left[\frac{\mathbf{E}\cdot(K\nabla\varepsilon - \varepsilon\nabla K)}{K + i\varepsilon\omega}\mathbf{E}^*\right] - \frac{1}{4}|\mathbf{E}|^2\nabla\varepsilon, \tag{34}$$

Re[...] stands for real part, and * for complex conjugate.

The local electrical conductivity is known through the ion concentrations (Eq. (9)). Gradients in conductivity can appear because there are ion concentration gradients: for instance, at the interface between two phases with different concentrations, or generated by Faradaic reactions that can produce concentration polarization. Gradients in conductivity can also occur because ion mobility is a function of temperature, so that we have $K = K(T)$.

In the case of ion concentration gradients, a conduction model with two species is useful to obtain a conservation equation for conductivity under iso-thermal conditions:

$$\frac{\partial K}{\partial t} + \mathbf{u}\cdot\nabla K = D\nabla^2 K, \tag{35}$$

where D is the ambipolar diffusion coefficient (Newman & Thomas-Alyea, 2004).

If the temperature field generates gradients in conductivity and permittivity, $\nabla K = (dK/dT)\nabla T$ and $\nabla\varepsilon = (d\varepsilon/dT)\nabla T$ must be used in Eq. (34). The required equation for temperature comes from the energy equation with a source term given by Joule heating. In steady conditions, the time-averaged temperature equation is (Ramos et al., 1998)

$$\kappa\nabla^2 T + K\langle E^2\rangle = 0, \tag{36}$$

where κ is the thermal conductivity.

7.1.2. Boundary conditions

Here we discuss those boundary conditions that are more relevant.

Electrical: When the microelectrodes are inside the channel, it is important to consider the polarization of the electrodes. For small voltages across the double layer, the interface metal-electrolyte can often be considered perfectly polarizable and the boundary condition is (González, Ramos, Green, Castellanos, and Morgan, 2000)

$$K\frac{\partial\Phi}{\partial n} = i\omega C_{DL}(\Phi - V), \tag{37}$$

where Φ is the liquid potential on the liquid side, n is the direction normal to the interface, C_{DL} is the double layer capacitance, and V is the potential on the metal. This boundary condition expresses the conservation of charge: the current arriving from the liquid bulk charges the double layer capacitor. It provides a characteristic frequency of transition $\omega_0 = K/C_{DL}\ell$. For $\omega \ll \omega_0$, the applied voltage is mainly dropped across the double layer, and for $\omega \gg \omega_0$ there is electric field in the bulk.

For the interface between two immiscible fluids, the equation of conservation of charge (16) must be considered. If the interface mechanical time is long compared to the period of the AC signal, a simplified boundary condition is

$$(K_1 + i\varepsilon_1\omega)E_{1n} = (K_2 + i\varepsilon_2\omega)E_{2n}, \tag{38}$$

which expresses the continuity of total current, ohmic plus displacement, across the interface. It is to be noticed that in the general case of a moving free surface, phasors for the electrical problem cannot be used. Only when the signal period is much shorter than the mechanical time of the interface, phasor notation can be employed.

Mechanical: For rigid boundaries, the nonslip condition usually applies. However, for polarizable surfaces like the electrode-electrolyte interface, there are forces in the double layer that generate electroosmotic slip, and the boundary condition becomes (Green, Ramos, Gonzalez, Morgan, & Castellanos, 2002)

$$u_{slip} = \frac{\varepsilon \langle E_t \Gamma \Delta\Phi \rangle}{\mu} = \frac{\varepsilon \Lambda}{2\mu} \mathrm{Re}[E_t \Delta\Phi^*], \tag{39}$$

where $\Delta\Phi = \Phi - V$ and Γ is a parameter that relates the diffuse layer potential to the total double layer (DL) potential. For $\omega \gg \omega_0$, the slip velocity goes to zero as the potential across the DL.

7.1.3. Examples of flows induced by AC fields

Electrical forces in the bulk: Electrothermal flows can be generated by the combination of AC electric fields and illumination (González, Ramos, Morgan, Green, & Castellanos, 2006). Light heating the electrodes creates a temperature field that generates permittivity and conductivity gradients. A rotating electric field produced by a four-phase AC signal was able to generate rotating flow (González et al., 2006). The rotating flow was maximum at a characteristic frequency of the order of the reciprocal charge relaxation time $f \sim K/(2\pi\varepsilon)$, as predicted. This mechanism has been employed to manipulate and concentrate colloidal particles near an electrode surface illuminated with a laser beam (Kumar et al., 2010).

Two-phase flows with a diffuse interface have been manipulated using AC fields (Morgan, Green, Ramos, & García-Sánchez, 2007). Coflowing streams of two electrolytes with different conductivities in a microchannel could be deflected by using AC electric fields. In this case, there is not a sharp interface but a smooth change of electrical conductivity that can be described by the convection-diffusion Eq. (35). Numerical simulations successfully explained the experimental observations (García-Sánchez, Ren, Arcenegui, Morgan, & Ramos, 2012). Extensive studies on the electrohydrodynamic instabilities of coflowing streams subject to DC electric fields have been performed by Chen, Lin, Lele, and Santiago (2005). They employed the diffusion equation for conductivity, and very good agreement was found between theory and experiments. The extension of these studies to AC fields is an interesting subject of research.

Electrical forces at the interface: Here we can differentiate flows where the electrokinetic effects at the double layer are important from those where the force is applied on the charges accumulated at the interface (the Debye layer) but the complications of electrokinetic equations are not required. In the first case, we can cite AC electroosmotic flows: flows driven by forces in the double layer of the electrode-electrolyte interface (Green, Ramos, Gonzalez, Morgan, & Castellanos, 2000). An example of the second case is the control of a sharp interface by AC fields, such as a jet in a microfluidic flow-focusing junction (Castro-Hernández et al., 2015).

AC electroosmotic flows (also known as induced charge electroosmotic flows) (Bazant and Squires, 2004) appear from the accumulation of counter-ions in the diffuse double layer and the action of the tangential component of the electric field on this charge. The AC potential applied at electrodes induces an oscillating charged layer on top of them that is actuated by the tangential component of the electric field. Both charged layer and tangential field are oscillating functions of time, thus producing steady and time-periodic forces. These forces generate slip velocity with steady and oscillating components. The one that is easily observed is the steady component (Green et al., 2000), and good agreement has been verified between theory and experiments (Green et al., 2002). AC electroosmosis has been demonstrated to be useful for the following applications in microfluidics: pumping (Brown, Smith, & Rennie, 2000), mixing (Harnett, Templeton, Dunphy-Guzman, Senousy, & Kanouff, 2008), concentration of molecules such as DNA (Lei, Cheng, Choy, & Chow, 2009).

The sharp interface between immiscible fluids can be actuated by AC fields (J. Melcher & G. Taylor, 1969). In microfluidics, AC electrified jets in a microfluidic flow-focusing junction have been produced with control of drop production and jet length by either voltage amplitude or frequency of the applied signal (Castro-Hernández et al., 2015, 2016).

7.2. AC electrospray

In contrast to the research on DC electrospray, there have been relatively few studies on AC electrospray. At very low frequencies, a behavior analogous to that for a changing DC field has been reported. Taylor cones are formed and terminated every half cycle. At signal frequencies coincident with natural frequencies of the meniscus, resonant deformation of the drops was observed, and at higher voltages transient Taylor cones appeared evenly distributed over the entire meniscus (Wang, Maheshwari, & Chang, 2006). For higher frequencies ($>10\ kHz$), greater than the frequency of drop production, Yeo et al. (2004) reported jetting behavior that is capable of generating micron-sized electroneutral drops. Increasing the frequency, they observed a change in the behavior of the meniscus at frequencies of the order of the charge relaxation frequency ($f = K/\varepsilon$). Beyond this frequency, wetting that drew the liquid up the needle was observed. The authors explained this change in behavior due to a change of the Maxwell-Wagner interfacial stress at the drop tip; that is to say, a change in the dipole induced at the drop as a function of frequency. The Maxwell-Wagner polarization frequency is related to the transition from the conductor to insulator behavior of the meniscus as the signal frequency becomes greater than the reciprocal of the charge relaxation time. In this range of high frequencies, the electric field amplitude becomes important inside the drop. This opens the door to the appearance of electrical forces inside the meniscus. In particular, flows as described previously could be generated close to the metal nozzle due to AC electric fields. The high frequency AC electrospray has been proposed as a fabrication method for biomaterials synthesis (L.Y. Yeo et al., 2005), with the advantage in front of DC electrospray of producing micron-sized drops which are typically larger and electroneutral.

Interestingly, there is a range of higher frequencies (from 10 to 200 kHz) and higher voltages (around 5 kV peak-to-peak) where AC electrospray shows the appearance of slender conical menisci (half angle around 10°) (Maheshwari & Chang, 2006). These cone angles are much smaller than Taylor's cone angle 49.3°. This regime happens for angular frequencies of the order of or greater than the reciprocal of the meniscus charge relaxation time (Chetwani et al., 2008b; Maheshwari & Chang, 2006). Although in DC experiments charged drops emitted from the cone can lead to a reduction of the cone angle (De La Mora, 1992), these angles are still far

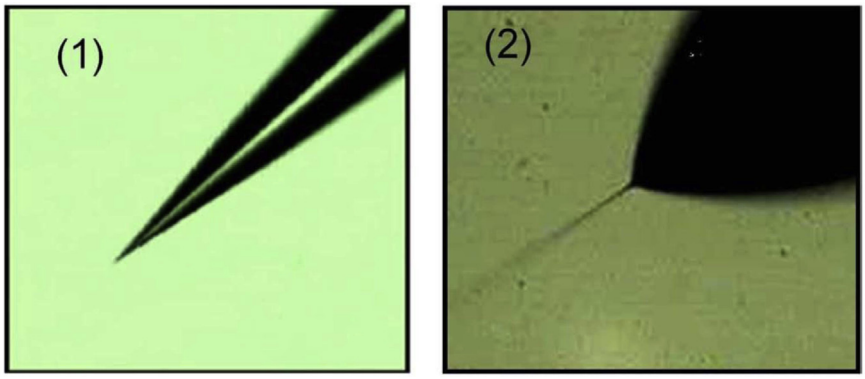

Fig. 13. (1) AC and (2) DC cone-jets of ethanol. From Ref. N. Chetwani, C.A. Cassou, D.B. Go, and H.-C. Chang (2010b) (with permission).

from the cone angles around 10° observed in AC electrospray (see Fig. 13). These AC conical tips have been proposed as ionization sources for mass spectrometry of biomolecules (Chetwani et al., 2010b). According to Chetwani et al. (2008b), the conical tips are originated by a buildup of space charge in the cone because of insufficient time to relax onto the surface of low mobility ions at these high frequencies. The resulting Coulombic repulsion sustains the AC cone. An alternative explanation is that there exist steady solutions of conical tips for ohmic liquids in AC electric fields (Demekhin, Polyanskikh, & Ramos, 2011). These steady solutions for ohmic liquids are an extension to the AC case of Taylor's solution for conducting drops (Taylor, 1964) and the conical solutions for purely dielectric drops (Ramos & Castellanos, 1994, Li, Halsey, & Lobkovsky, 1994). The theoretical cone angles can be very small for signal frequencies of the order of the reciprocal charge relaxation time, and they may correspond to the experimental observations for AC fields.

Most of the theoretical approaches to understand the behavior of AC electrospray employ the leaky dielectric model, where materials are characterized by their conductivity K and permittivity ε. As explained in Section 3, in this model electrical charges are mainly superficial, placed at interfaces between different phases. This model was used by Yeo et al. (2004) to explain the transitions of the jetting behavior. It was also used by Demekhin et al. (2011) to obtain conical solutions as a function of frequency, which could conform the slender conical tips observed experimentally. The boundary condition (38) of continuity of total normal current is used at a conical interface in order to look for electric fields with singular solutions that go as $r^{-1/2}$, where r is the distance to the cone vertex. Reference (Chetwani et al., 2008b) departs from the ohmic model and considers space charge at the tip in order to explain the observations. It would be interesting to investigate the effect of charge in a finite Debye layer using the electrokinetic equations, which could be important near these conical points.

8. Conclusion

To summarize, we have comprehensively reviewed the physics of liquid ejection by the application of electric fields. We have considered the full electrokinetic equations to briefly explain how they can be simplified into the Taylor-Melcher leaky dielectric model. This model constitutes a very useful theoretical framework to analyze electrohydrodynamic phenomena, especially the steady cone-jet mode of electrospray. We have extensively reviewed this operation mode, considering its predicting scaling laws and stability. The extension of Taylor cone-jets to coaxial and AC electrospraying is also reviewed. This latter phenomenon has been put in context by deriving the equations for AC electrohydrodynamics.

Electrospray as a scientific and technological keyword has undergone a mild decrease in publications since about five years ago, which shows the conversion of electrospray from a fertile area of scientific curiosity to a mature standard tool for several fundamental applications (e.g. mass spectrometry of large biomolecules, thin-film deposition, etc.). Yet, it still offers one of the most complex and multidisciplinary macroscale phenomena that one may find in Physics for further scientific insight. In particular, the global stability analysis of the Taylor cone-jet is still unexplored, as it is the scaling laws of the nano-electrospray emissions. Finally, the emission characteristics of Taylor cone-jets in the presence of electrical discharges (e.g. Borra et al., 1999, 2004), not reviewed in this work, still offers an ample fertile field for further research and applications.

Acknowledgements

This work has been supported by the Spanish Ministry of Economy, Industry and Competitiveness under grant DPI2016-78887. We are grateful to Prof. Jean-Pascal Borra for useful comments and suggestions.

References

Ahmad, Z., Zhang, H., Farook, U., Edirisinghe, M., Stride, E., & Colombo, P. (2008). Generation of multilayered structures for biomedical applications using a novel tri-needle coaxial device and electrohydrodynamic flow. *Journal of the Royal Society Interface, 5*(27), 1255–1261.

Artana, G., Touchard, G., & Romat, H. (1997). Absolute and convective instabilities in an electrified jet. *Journal of Electrostatics, 40–41*, 33–38.

Barenblatt, G. I. (2003). *Scaling*. Cambridge, UK: Cambridge University Press.
Barrero, A., Gañán-Calvo, A. M., Dávila, J., Palacio, A., & Gómez-González, E. (1998). Low and high Reynolds number flows inside Taylor cones. *Physical Review E, 58*, 7309–7314.
Basset, E. B. (1894). Waves and jets in a viscous liquid. *American Journal of Mathmatics, 16*, 93–110.
Baygents, J.C., & Saville, D.A. (1989). The circulation produced in a drop by an electric field: a high field strength electrokinetic model. In Wang, T. (Ed.), AIP Conference Proceedings, vol. 7, American Institute of Physics, 7–17.
Bazant, M. Z. (2015). Electrokinetics meets electrohydrodynamics. *Journal of Fluid Mechanics, 782*, 1–4.
Bazant, M. Z., & Squires, T. M. (2004). Induced-charge electrokinetic phenomena: Theory and microfluidic applications. *Physical Review Letters, 92*(6), 066101.
Bird, R. B., Armstrong, R. C., & Hassager, O. (1987). *Dynamics of polymeric liquids*. United States of America: John Wiley & Sons, Inc.
Borra, J.-P., Ehouarn, P., & Boulaud, D. (2004). Electrohydrodynamic atomisation of water stabilised by glow discharge - Operating range and droplet properties. *Journal of Aerosol Science, 35*(11), 1313–1332.
Borra, J.-P., Hartmann, R., Marijnissen, J., & Scarlett, B. (1996). Destabilisation of sprays in the cone-jet mode by electrical dicharges on the jet. *Journal of Aerosol Science, 27*(SUPPL.1), S203–S204.
Borra, J.-P., Tombette, Y., & Ehouarn, P. (1999). Influence of electric field (symmetry, intensity and divergent) on the mode of EHD: Pulverization of liquids related to discharge regimes. *Journal of Aerosol Science, 30*(7), 913–925.
Brosseau, Q., & Vlahowska, P. M. (2017). Streaming from the equator of a drop in an external electric field. *Physical Review Letters, 119*, 034501.
Brown, A., Smith, C., & Rennie, A. (2000). Pumping of water with ac electric fields applied to asymmetric pairs of microelectrodes. *Physical Review E, 63*(1), 016305.
Carroll, C. P., & Joo, Y. L. (2008). Axisymmetric instabilities of electrically driven viscoelastic jets. *Journal of Non-Newtonian Fluid Mechanics, 153*, 130–148.
Castellanos, A., Ramos, A., Gonzalez, A., Green, N. G., & Morgan, H. (2003). Electrohydrodynamics and dielectrophoresis in microsystems: Scaling laws. *Journal of Physics D: Applied Physics, 36*(20), 2584.
Castro-Hernández, E., García-Sánchez, P., Alzaga-Gimeno, J., Tan, S. H., Baret, J.-C., & Ramos, A. (2016). AC electrified jets in a flow-focusing device: Jet length scaling. *Biomicrofluidics, 10*(4), 043504.
Castro-Hernández, E., García-Sánchez, P., Tan, S. H., Gañán-Calvo, A. M., Baret, J.-C., & Ramos, A. (2015). Breakup length of AC electrified jets in a microfluidic flow-focusing junction. *Microfluidics and Nanofluidics, 19*(4), 787–794.
Chen, C.-H., Lin, H., Lele, S. K., & Santiago, J. G. (2005b). Convective and absolute electrokinetic instability with conductivity gradients. *Journal of Fluid Mechanics, 524*, 263–303.
Chen, C.-H., Saville, D. A., & Aksay, I. A. (2006). Scaling laws for pulsed electrohydrodynamic drop formation. *Applied Physics Letters, 89*, 124103.
Chen, D.-R., Pui, D. Y. H., & Kaufman, S. L. (1995). Electrospraying of conducting liquids for monodisperse aerosol generation in the 4 nm to 1.8 μm diameter range. *Journal of Aerosol Science, 26*, 963–977.
Chen, H., Zhao, Y., Song, Y., & Jiang, L. (2008). One-step multicomponent encapsulation by compound-fluidic electrospray. *Journal of the American Chemical Society, 130*(25), 7800–7801.
Chen, X., Jia, L., Yin, X., Cheng, J., & Lu, J. (2005). Spraying modes in coaxial jet electrospray with outer driving liquid. *Physics of Fluids, 17*(3), 032101.
Cherney, L. T. (1999). Structure of Taylor cone-jets: Limit of low flow rates. *Journal of Fluid Mechanics, 378*, 167–196.
Chetwani, N., Cassou, C., Go, D., & Chang, H.-C. (2010a). High-frequency AC electrospray ionization source for mass spectrometry of biomolecules. *Journal of the American Society for Mass Spectrometry, 21*(11), 1852–1856.
Chetwani, N., Cassou, C., Go, D., & Chang, H.-C. (2011). Frequency dependence of alternating current electrospray ionization mass spectrometry. *Analytical Chemistry, 83*(8), 3017–3023.
Chetwani, N., Cassou, C. A., Go, D. B., & Chang, H.-C. (2010b). High-frequency AC electrospray ionization source for mass spectrometry of biomolecules. *Journal of the American Society for Mass Spectrometry, 21*(11), 1852–1856.
Chetwani, N., Maheshwari, S., & Chang, H.-C. (2008a). Universal cone angle AC electrosprays due to net charge entrainment. *Physical Review Letters, 101*(20), 204501.
Chetwani, N., Maheshwari, S., & Chang, H.-C. (2008b). Universal cone angle of ac electrosprays due to net charge entrainment. *Physical Review Letters, 101*(20), 204501.
Chiarot, P. R., Gubarenko, S. I., Mrad, R. B., & Sullivan, P. (2009). On the pulsed and transitional behavior of an electrified fluid interface. *Journal of Fluid Engineering, 131*, 091202.
Choi, D., Park, C., Kim, I., Chun, H., Park, K., & Han, D. (2010). Fabrication of core-shell microcapsules using PLGA and alginate for dual growth factor delivery system. *Journal of Controlled Release, 147*(2), 193–201.
Clasen, C., Plog, J. P., Kulicke, W.-M., Owens, M., Macosko, C., Scriven, L. E., ... McKinley, G. H. (2006). How dilute are dilute solutions in extensional flows? *Journal of Rheology, 50*, 849–881.
Cloupeau, M., & Prunet-Foch, B. (1989). Electrostatic spraying of liquids in cone-jet mode. *Journal of Electrostatics, 22*, 135–159.
Cloupeau, M., & Prunet-Foch, B. (1994). Electrohydrodynamic spraying functioning modes: A critical review. *Journal of Aerosol Science, 25*, 1021–1036.
Collins, R. T., Harris, M. T., & Basaran, O. A. (2007). Breakup of electrified jets. *Journal of Fluid Mechanics, 588*, 75–129.
Collins, R. T., Jones, J. J., Harris, M. T., & Basaran, O. A. (2008). Electrohydrodynamic tip streaming and emission of charged drops from liquid cones. *Nature Physics, 4*, 149–154.
Collins, R. T., Sambath, K., Harris, M. T., & Basaran, O. A. (2013). Universal scaling laws for the disintegration of electrified drops. *Proceedings of the National Academy of Sciences of the USA, 110*, 4905–4910.
Conroy, D. T., Matar, K., Craster, R. V., & Papageorgiou, D. T. (2011). Breakup of an electrified viscous thread with charged surfactants. *Physics of Fluids, 23*, 022103.
Cruz-Mazo, F., Montanero, J. M., & Gañán-Calvo, A. (2016). Monosized dripping mode of axisymmetric flow focusing. *Physical Review E, 94*(5), 053122.
Fernandez de la Mora, J. (1992). The effect of charge emission from electrified liquid cones. *Journal of Fluid Mechanics, 243*, 561–574.
Demekhin, E., Polyanskikh, S., & Ramos, A. (2011). Taylor cones in a leaky dielectric liquid under an ac electric field. *Physical Review E, 84*(3), 035301.
Duft, D., Achtzehn, T., Müller, R., Huber, B., & Leisner, T. (2003). Coulomb fission: Rayleigh jets from levitated microdroplets. *Nature, 421*(6919), 128.
Eggers, J. (1993). Universal pinching of 3D axisymmetric free-surface flow. *Physical Review Letters, 71*, 3458–3460.
Eggers, J., & Dupont, T. F. (1994). Drop formation in a one-dimensional approximation of the Navier-Stokes equation. *Journal of Fluid Mechanics, 262*, 205–221.
Eggers, J., & Villermaux, E. (2008). Physics of liquid jets. *Reports on Progress in Physics, 71*, 036601.
Fernandez de la Mora, J., & Loscertales, I. G. (1994). The current transmitted through an electrified conical meniscus. *Journal of Fluid Mechanics, 260*, 155–184.
Fernández de la Mora, J. (2007). The fluid dynamics of Taylor Cones. *Annual Review of Fluid Mechanics, 39*, 217–243.
Gamero-Castaño, M. (2008aa). Characterization of the electrosprays of 1-ethyl-3-methylimidazolium bi(trifluoromethylsulfonyl)imide in vacuum. *Physics of Fluids, 20*, 1–11 (032103).
Gamero-Castaño, M. (2008bb). The structure of electrospray beams in vacuum. *Journal of Fluid Mechanics, 604*, 339–368.
Gamero-Castaño, M. (2010). Energy dissipation in electrosprays and the geometric scaling of the transition region of cone-jets. *Journal of Fluid Mechanics, 662*, 493–513.
Gamero-Castaño, M., & Hruby, V. (2002). Electric measurements of charged sprays emitted by cone-jets. *Journal of Fluid Mechanics, 459*, 245–276.
Gañán-Calvo, A., López-Herrera, J. M., Rebollo-Muñoz, N., & Montanero, J. M. (2016). The onset of electrospray: The universal scaling laws of the first ejection. *Scientific Reports, 6*, 32357.
Gañán-Calvo, A. M. (1997). Cone-Jet analytical extension of taylor's electrostatic solution and the asymptotic universal scaling laws in electrospraying. *Physical Review Letters, 79*, 217–220.
Gañán-Calvo, A. M. (1998). Generation of steady liquid microthreads and micron-sized monodisperse sprays in gas streams. *Physical Review Letters, 80*, 285–288.
Gañán-Calvo, A. M. (1999). The surface charge in electrospraying: Its nature and its universal scaling laws. *Journal of Aerosol Science, 30*, 863–872.
Gañán-Calvo, A. M. (2004). On the general scaling theory for electrospraying. *Journal of Fluid Mechanics, 507*, 203–212.
Gañán-Calvo, A. M., Barrero, A., & Pantano, C. (1993). The electrohydrodynamics of electrified conical menisci. *Journal of Aerosol Science, 24*, S19–20.

Gañán-Calvo, A. M., Dávila, J., & Barrero, A. (1997). Current and droplet size in the electrospraying of liquids. Scaling laws. *Journal of Aerosol Science, 28*, 249–275.
Gañán-Calvo, A. M., Lasheras, J. C., Dávila, J., & Barrero, A. (1994). The electrostatic spray emitted from an electrified conical meniscus. *Journal of Aerosol Science, 25*, 1121–1142.
Gañán-Calvo, A. M., & Montanero, J. M. (2009). Revision of capillary cone-jet physics: Electrospray and flow focusing. *Physical Review E, 79*, 066305.
Gañán-Calvo, A. M., Rebollo-Muñoz, N., & Montanero, J. M. (2013). Physical symmetries and scaling laws for the minimum or natural rate of flow and droplet size ejected by Taylor cone-jets. *New Journal of Physics, 15*, 033035.
García-Sánchez, P., Ren, Y., Arcenegui, J. J., Morgan, H., & Ramos, A. (2012). Alternating current electrokinetic properties of gold-coated microspheres. *Langmuir, 28*(39), 13861–13870.
Garoz, D., Bueno, C., Larriba, C., Castro, S., Romero-Sanz, I., de la Mora, J. F., ... Saito, G. (2007). Taylor cones of ionic liquids from capillary tubes as sources of pure ions: The role of surface tension and electrical conductivity. *Journal of Applied Physics, 102*, 064913.
Gomez, A., & Tang, K. (1994). Charge and fission of droplets in electrostatic sprays. *Physics of Fluids, 6*(1), 404–414.
Gonzalez, A., Ramos, A., Green, N., Castellanos, A., & Morgan, H. (2000). Fluid flow induced by nonuniform ac electric fields in electrolytes on microelectrodes. II. Linear double-layered analysis. *Physical Review E, 61*(4), 4019.
González, A., Ramos, A., Morgan, H., Green, N. G., & Castellanos, A. (2006). Electrothermal flows generated by alternating and rotating electric fields in microsystems. *Journal of Fluid Mechanics, 564*, 415–433.
Green, N., Ramos, A., Gonzalez, A., Morgan, H., & Castellanos, A. (2000). Fluid flow induced by nonuniform ac electric fields in electrolytes on microelectrodes. I. Experimental measurements. *Physical Review E, 61*(4), 4011.
Green, N. G., Ramos, A., Gonzalez, A., Morgan, H., & Castellanos, A. (2002). Fluid flow induced by nonuniform ac electric fields in electrolytes on microelectrodes. III. Observation of streamlines and numerical simulation. *Physical Review E, 66*(2), 026305.
Greiner, A. (2007). A fascinating method for the preparation of ultrathin fibers. *Angewandte Chemie - International Edition, 46*(30), 5670–5703.
Grifoll, J., & Rosell-Llompart, J. (2012). Efficient Lagrangian simulation of electrospray droplets dynamics. *Journal of Aerosol Science, 47*, 78–93.
Harnett, C. K., Templeton, J., Dunphy-Guzman, K. A., Senousy, Y. M., & Kanouff, M. P. (2008). Model based design of a microfluidic mixer driven by induced charge electroosmosis. *Lab on a Chip, 8*(4), 565–572.
Hartman, R., Borra, J.-P., Brunner, D., Marijnissen, J., & Scarlett, B. (1999b). The evolution of electrohydrodynamic sprays produced in the cone-jet mode, a physical model. *Journal of Electrostatics, 47*(3), 143–170.
Hartman, R. P. A., Brunner, D. J., Camelot, D. M. A., Marijnissen, J. C. M., & Scarlett, B. (1999a). Electrohydrodynamic atomization in the cone-jet mode physical modeling of the liquid cone and jet. *Journal of Aerosol Science, 30*, 823–849.
Hartman, R. P. A., Brunner, D. J., Camelot, D. M. A., Marijnissen, J. C. M., & Scarlett, B. (2000). Jet Break-up in Electrohydrodynamic atomization in the Cone-jet Mode. *Journal of Aerosol Science, 31*, 65–95.
Hayati, I., Bailey, A. I., & Tadros, T. F. (1987aa). Investigations into the mechanism of electrohydrodynamic spraying of liquids: II. Mechanism of stable jet formation and electrical forces acting on a liquid cone. *Journal of Colloid Interface Science, 117*, 222–230.
Hayati, I., Bailey, A. I., & Tadros, T. F. (1987bb). Investigations into the mechanism of electrohydrodynamic spraying of liquids: I. Effect of Electric Field and the Environment on Pendant Drops and Factors Affecting the Formation of Stable Jets and Atomization. *Journal of Colloid Interface Science, 117*, 202–221.
Haywood, D., Saha-Shah, A., Baker, L., & Jacobson, S. (2015). Fundamental studies of nanofluidics: Nanopores, nanochannels, and nanopipets. *Analytical Chemistry, 87*(1), 172–187.
Herrada, M. A., López-Herrera, J. M., Gañán-Calvo, A. M., Vega, E. J., Montanero, J. M., & Popinet, S. (2012). Numerical simulation of electrospray in the cone-jet mode. *Physical Review E, 86*, 026305.
Herrada, M. A., & Montanero, J. M. (2016). A numerical method to study the dynamics of capillary fluid systems. *Journal of Computational Physics, 306*, 137–147.
Higuera, F. J. (2010). Numerical computation of the domain of operation of an electrospray of a very viscous liquid. *Journal of Fluid Mechanics, 648*, 35–52.
Higuera, F. J. (2017). Qualitative analysis of the minimum flow rate of a cone-jet of a very polar liquid. *Journal of Fluid Mechanics, 816*, 428–441.
Hijano, A. J., Loscertales, I. G., Ibáñez, S. E., & Higuera, F. J. (2015). Periodic emission of droplets from an oscillating electrified meniscus of a low-viscosity, highly conductive liquid. *Physical Review E, 91*, 013011.
Huang, Z.-M., He, C.-L., Yang, A., Zhang, Y., Han, X.-J., Yin, J., & Wu, Q. (2006). Encapsulating drugs in biodegradable ultrafine fibers through co-axial electrospinning. *Journal of Biomedical Materials Research - Part A, 77*(1), 169–179.
Huerre, P., & Monkewitz, P. A. (1990). Local and global instabilites in spatially developing flows. *Annual Review of Fluid Mechanics, 22*, 473–537.
James, D. F. (2009). Boger fluids. *Annual Review of Fluid Mechanics, 41*, 129–142.
Jaworek, A., & Krupa, A. (1999). Classification of the modes of EHD spraying. *Journal of Aerosol Science, 30*, 873–893.
Jaworek, A., Sobczyk, A., Czech, T., & Krupa, A. (2014). Corona discharge in electrospraying. *Journal of Electrostatics, 72*(2), 166–178.
Jidenko, N., Petit, M., & Borra, J. (2006). Electrical characterization of microdischarges produced by dielectric barrier discharge in dry air at atmospheric pressure. *Journal of Physics D: Applied Physics, 39*(2), 281–293.
Juraschek, R., & Röllgen, F. (1998). Pulsation phenomena during electrospray ionization. *International Journal of Mass Spectrometry, 177*(1), 1–15.
Kim, H., Teramoto, Y., Negishi, N., Ogata, A., Kim, J., Pongrác, B., ... Gañán-Calvo, A. M. (2014). Polarity effect on the electrohydrodynamic (EHD) spray of water. *Journal of Aerosol Science, 76*, 98–114.
Kumar, A., Kwon, J.-S., Williams, S. J., Green, N. G., Yip, N. K., & Wereley, S. T. (2010). Optically modulated electrokinetic manipulation and concentration of colloidal particles near an electrode surface. *Langmuir, 26*(7), 5262–5272.
Larriba, C., & Fernandez de la Mora, J. (2011). Production of monodisperse submicron drops of dielectric liquids by charge-injection from highly conducting liquids. *Physics of Fluids, 23*(10), 102003.
Lei, K. F., Cheng, H., Choy, K. Y., & Chow, L. M. (2009). Electrokinetic DNA concentration in microsystems. *Sensors and Actuators A: Physical, 156*(2), 381–387.
Leib, S. J., & Goldstein, M. E. (1986). Convective and absolute instability of a viscous liquid jet. *Physics of Fluids, 29*, 952–954.
Li, D., & Xia, Y. (2004). Electrospinning of nanofibers: Reinventing the wheel? *Advanced Materials, 16*(14), 1151–1170.
Li, F., Gañán-Calvo, A. M., & López-Herrera, J. M. (2011a). Absolute-convective instability transition of low permittivity, low conductivity charged viscous liquid jets under axial electric fields. *Physics of Fluids, 23*, 094108.
Li, F., Gañán-Calvo, A. M., López-Herrera, J. M., Yin, X.-Y., & Yin, X.-Z. (2013). Absolute and convective instability of a charged viscoelastic liquid jet. *Journal of Non-Newtonian Fluid Mechanics, 196*, 58–69.
Li, F., Yin, X.-Y., & Yin, X.-Z. (2006). Linear instability of a coflowing jet under an axial electric field. *Physical Review E, 74*, 036304.
Li, F., Yin, X.-Y., & Yin, X.-Z. (2008). Instability of a viscous coflowing jet in a radial electric field. *Journal of Fluid Mechanics, 596*, 285–311.
Li, F., Yin, X.-Y., & Yin, X.-Z. (2009). Axisymmetric and non-axisymmetric instability of an electrified viscous coaxial jet. *Journal of Fluid Mechanics, 632*, 199–225.
Li, F., Yin, X.-Y., & Yin, X.-Z. (2011b). Axisymmetric and non-axisymmetric instability of an electrically charged viscoelastic liquid jet. *Journal of Non-Newtonian Fluid Mechanics, 166*, 1024–1032.
Li, H., Halsey, T. C., & Lobkovsky, A. (1994). Singular shape of a fluid drop in an electric or magnetic field. *EPL (Europhysics Letters), 27*(8), 575–580.
López-Herrera, J. M., Barrero, A., López, A., Loscertales, I., & Márquez, M. (2003). Coaxial jets generated from electrified Taylor cones. Scaling laws. *Journal of Aerosol Science, 34*, 535–552.
López-Herrera, J. M., Barrero, A., Boucard, A., Loscertales, I. G., & Márquez, M. (2004). An experimental study of the electrospraying of water in air at atmospheric pressure. *Journal of the American Society for Mass Spectrometry, 15*, 253–259.
López-Herrera, J. M., Gañán-Calvo, A., Popinet, S., & Herrada, M. A. (2015). Electrokinetic effects in the breakup of electrified jets: A Volume-Of-Fluid numerical study. *International Journal of Multiphase Flow, 71*, 14–21.
López-Herrera, J. M., & Gañán-Calvo, A. M. (2004). A note on charged capillary jet breakup of conducting liquids: Experimental validation of a viscous one-dimensional model. *Journal of Fluid Mechanics, 501*, 303–326.
López-Herrera, J. M., Gañán-Calvo, A. M., & Herrada, M. A. (2010). Absolute to convective instability transition in charged liquid jets. *Physics of Fluids, 22*, 062002.

López-Herrera, J. M., Herrada, M. A., Montanero, J. M., Rebollo-Muñoz, N., & Gañán-Calvo, A. M. (2013). On the validity and applicability of the one-dimensional approximation in cone-jet electrospray. *Journal of Aerosol Science, 61*, 60–69.

López-Herrera, J. M., Riesco-Chueca, P., & Gañán-Calvo, A. M. (2005). Linear stability analysis of axisymmetric perturbations in imperfectly conducting liquid jets. *Physics of Fluids, 17*, 034106.

Loscertales, I. G., Barrero, A., Guerrero, I., Cortijo, R., Marquez, M., & Gañán-Calvo, A. M. (2002). Micro/Nano encapsulation via electrified coaxial liquid jets. *Science, 295*, 1695–1698.

Maheshwari, S., & Chang, H.-C. (2006). Anomalous conical menisci under an ac field-departure from the dc Taylor cone. *Applied Physics Letters, 89*(23), 234103.

Maheshwari, S., & Chang, H.-C. (2009). Assembly of multi-stranded nanofiber threads through AC electrospinning. *Advanced Materials, 21*(3), 349–354.

Manz, A., Harrison, D. J., Verpoorte, E. M., Fettinger, J. C., Paulus, A., Lüdi, H., & Widmer, H. M. (1992). Planar chips technology for miniaturization and integration of separation techniques into monitoring systems: Capillary electrophoresis on a chip. *Journal of Chromatography A, 593*(1–2), 253–258.

Marín, A. G., Loscertales, I. G., Márquez, M., & Barrero, A. (2007). Simple and double emulsions via coaxial jet electrosprays. *Physical Review Letters, 98*, 014502.

Melcher, J., & Taylor, G. (1969b). Electrohydrodynamics: A review of the role of interfacial shear stresses. *Annual Review of Fluid Mechanics, 1*(1), 111–146.

Melcher, J. R., & Taylor, G. I. (1969a). Electrohydrodynamics: A review of the role of interfacial shear stresses. *Annual Review of Fluid Mechanics, 1*, 111–146.

Mestel, A. J. (1994). Electrohydrodynamic stability of a slightly viscous jet. *Journal of Fluid Mechanics, 274*, 93–113.

Mestel, A. J. (1996). Electrohydrodynamic stability of a highly viscous jet. *Journal of Fluid Mechanics, 312*, 311–326.

Montanero, J. M., Rebollo-Muñoz, N., Herrada, M. A., & Gañán-Calvo, A. M. (2011). Global stability of the focusing effect of fluid jet flows. *Physical Review E, 83*, 036309.

Morelle, W., & Michalski, J.-C. (2007). Analysis of protein glycosylation by mass spectrometry. *Nature Protocols, 2*(7), 1585–1602.

Morgan, H., Green, N. G., Ramos, A., & García-Sánchez, P. (2007). Control of two-phase flow in a microfluidic system using ac electric fields. *Applied Physics Letters, 91*(25), 254107.

Newman, J., & Thomas-Alyea, K. E. (2004). *Electrochemical systems.* John Wiley & Sons.

Pantano, C., Gañán-Calvo, A. M., & Barrero, A. (1994). Zeroth-Order, electrohydrostatic solution for electrospraying in cone-jet mode. *Journal of Aerosol Science, 25*, 1065–1077.

Park, J.-H., & Braun, P. (2010). Coaxial electrospinning of self-healing coatings. *Advanced Materials, 22*(4), 496–499.

Pillai, R., Berry, J. D., Harvie, D. J. E., & Davidson, M. R. (2016). Electrokinetics of isolated electrified drops. *Soft Matter, 12*, 3310–3325.

Pohl, H. A. (1978). *Dielectrophoresis: The behavior of neutral matter in nonuniform electric fields. 80*. Cambridge: Cambridge university press.

Ponce-Torres, A., Montanero, J. M., Herrada, M. A., Vega, E. J., & Vega, J. M. (2017). Influence of the surface viscosity on the breakup of a surfactant-laden drop. *Physical Review Letters, 118*, 024501.

Pongrác, B., Krcma, F., Dostál, L., Kim, H.-H., Homola, T., & Machala, Z. (2016). Effects of corona space charge polarity and liquid phase ion mobility on the shape and velocities of water jets in the spindle jet and precession modes of water electro-spray. *Journal of Aerosol Science, 101*, 196–206.

Ramos, A., & Castellanos, A. (1994). Conical points in liquid-liquid interfaces subjected to electric fields. *Physics Letters A, 184*(3), 268–272.

Ramos, A., Morgan, H., Green, N. G., & Castellanos, A. (1998). Ac electrokinetics: A review of forces in microelectrode structures. *Journal of Physics D: Applied Physics, 31*(18), 2338.

Rayleigh, J.W.S., On the Equilibrium of Liquid Conducting masses charged with electricity, Prec.Roy. Soc. 5, 1881, 110.

Rebollo-Muñoz, N. (2013). Análisis experimental de procesos de atomización de líquidos basados en campos hidrodinámicos y electrohidrodinámicos (Thesis). Universidad de Extremadura, Badajoz, Spain.

Reneker, D. H., & Yarin, A. L. (2008). Electrospinning jets and polymer nanofibers. *Polymer, 49*, 2387–2425.

Reznik, S. N., Yarin, A. L., Theron, A., & Zussman, E. (2004). Transient and steady shapes of droplets attached to a surface in a strong electric field. *Journal of Fluid Mechanics, 516*, 349–377.

Reznik, S. N., Yarin, A. L., Zussman, E., & Bercovici, L. (2006). Evolution of a compound droplet attached to a core-shell nozzle under the action of a strong electric field. *Physics of Fluids, 18*, 062101.

Rosell-Llompart, J., & de la Mora, J. F. (1994). Generation of monodisperse droplets 0.3 to 4 micrometre in diameter from electrified cone-jets of highly conducting and viscous liquids. *Journal of Aerosol Science, 25*, 1093–1119.

Rosell-Llompart, J. (1994), Yale University, Yale, USA.

Saha-Shah, A., Weber, A., Karty, J., Ray, S., Hieftje, G., & Baker, L. (2015). Nanopipettes: Probes for local sample analysis. *Chemical Science, 6*(6), 3334–3341.

Saville, D. A. (1997). ELECTROHYDRODYNAMICS: The Taylor-Melcher leaky dielectric model. *Annual Review of Fluid Mechanics, 29*, 27–64.

Scheideler, W. J., & Chena, C.-H. (2014). The minimum flow rate scaling of Taylor cone-jets issued from a nozzle. *Applied Physics Letters, 104*, 024103.

Schmid, P. J. (2007). Nonmodal stability theory. *Annual Review of Fluid Mechanics, 39*, 129–162.

Schnitzer, O., & Yariv, E. (2015). The Taylor-Melcher leaky dielectric model as a macroscale electrokinetic description. *Journal of Fluid Mechanics,* (2015), 1–33.

Shin, Y. M., Hohman, M. M., Brenner, M. P., & Rutledge, G. C. (2001). Experimental characterization of electrospinning: The electrically forced jet and instabilities. *Polymer, 42*, 9955–9967.

Smith, D. P. H. (1986). The electrohydrodynamic atomization of liquids. *IEEE Transactions on Industry Applications,* 527–535 (IA22).

Smith, K., Alexander, M., & Stark, J. (2006). Voltage effects on the volumetric flow rate in cone-jet mode electrospraying. *Journal of Applied Physics, 99*(6), 064909.

Stark, J., Alexander, M., & Smith, K. (2014). Electrospray pulsation: A diagnostic to understand cone-jet stability and minimum flow. *Applied Physics Letters, 115*, 044905.

Stone, H. A., Stroock, A. D., & Ajdari, A. (2004). Engineering flows in small devices: Microfluidics toward a lab-on-a-chip. *Annual Review of Fliud Mechanics, 36*, 381–411.

Stratton, J. A. (1941). *Electromagnetic theory.* McGraw-Hill.

Szostek, B., Zajac, J., & Koropchak, J. A. (1997). Coupling condensation nucleation light scattering detection with capillary electrophoresis using electrospray. *Analytical Chemistry, 69*, 2955–2962.

Tang, K., & Gomez, A. (1995). Generation of monodisperse water droplets from electrosprays in a corona-assisted cone-jet mode. *Journal of Colloid Interface Science, 175*(2), 326–332.

Taylor, G. (1964). Disintegration of water drops in electric field. *Proceedings of the Royal Society of London A, 280*, 383–397.

Taylor, G. (1969). Electrically driven jets. *Proceedings of the Royal Society of London A, 313*, 453–475.

Theofilis, V. (2011). Global linear instability. *Annual Review of Fluid Mechanics, 43*, 319–352.

Tomotika, S. (1935). On the instability of a cylindrical thread of a viscous liquid surrounded by another viscous fluid. *Proceedings of the Royal Society of London A, 150*, 322–337.

Tran, S. B. Q., Byun, D., Nguyen, V. D., & Kang, T. S. (2009). Liquid meniscus oscillation and drop ejection by ac voltage, pulsed dc voltage, and superimposing dc to ac voltages. *Physical Review E, 80*, 026318.

Tran, S. B. Q., Byun, D., Yudistira, H. T., & Oh, J. H. (2011). Semianalytical study of hemispherical meniscus oscillation with an anchored edge on a conductive flat plate under an ac electric field. *Physics of Fluids, 23*, 022006.

Valo, H., Peltonen, L., Vehviläinen, S., Karjalainen, M., Kostiainen, R., Laaksonen, T., & Hirvonen, J. (2009). Electrospray encapsulation of hydrophilic and hydrophobic drugs in poly(L-lactic acid) nanoparticles. *Small, 5*(15), 1791–1798.

Vega, E. J., Montanero, J. M., Herrada, M. A., & Gañán-Calvo, A. M. (2010). Global and local instability of flow focusing: The influence of the geometry. *Physics of Fluids, 22*, 064105.

Velásquez-García, L., Akinwande, A., & Martínez-Sánchez, M. (2006). A micro-fabricated linear array of electrospray emitters for thruster applications. *Journal of Microelectromechanical Systems, 15*(5), 1260–1271.

Vioque-Martínez, E. (2012). *Revisión de la teoría del electrospray y obtención de chorros estables con caudal mínimo (Master Thesis)*. Sevilla, Spain: Universidad de Sevilla.

Wang, P., Maheshwari, S., & Chang, H.-C. (2006). Polyhedra formation and transient cone ejection of a resonant microdrop forced by an ac electric field. *Physical*

Review Letters, 96(25), 254502.
Wang, Q. (2012). Breakup of a poorly conducting liquid thread subject to a radial electric field at zero Reynolds number. *Physics of Fluids, 24*, 102102.
Wilm, M., Shevchenko, A., Houthaeve, T., Breit, S., Schweigerer, L., Fotsis, T., & Mann, M. (1996). Femtomole sequencing of proteins from polyacrylamide gels by nano-electrospray mass spectrometry. *Nature, 379*(6564), 466–469.
Xie, J., Marijnissen, J., & Wang, C.-H. (2006). Microparticles developed by electrohydrodynamic atomization for the local delivery of anticancer drug to treat C6 glioma in vitro. *Biomaterials, 27*(17), 3321–3332.
Xie, J., Ng, W., Lee, L., & Wang, C.-H. (2008). Encapsulation of protein drugs in biodegradable microparticles by co-axial electrospray. *Journal of Colloid and Interface Science, 317*(2), 469–476.
Xie, L., Yang, L., Qin, L., & Fu, Q. (2017). Temporal instability of charged viscoelastic liquid jets under an axial electric field. *European Journal of Mechanics B/Fluids, 66*, 60–70.
Xu, Y., & Hanna, M. (2006). Electrospray encapsulation of water-soluble protein with polylactide. Effects of formulations on morphology, encapsulation efficiency and Release Profile of particles. *International Journal of Pharmaceutics, 320*(1–2), 30–36.
Yang, L., Liu, Y., & Fu, Q. (2012). Linear stability analysis of an electrified viscoelastic liquid jet. *Journal of Fluids Engineering, 134*, 071303.
Yang, W., Lu, Y., Xiang, Z., & Luo, G. (2007). Monodispersed microcapsules enclosing ionic liquid of 1-butyl-3-methylimidazolium hexafluorophosphate. *Reactive and Functional Polymers, 67*(1), 81–86.
Yeo, L., Gagnon, Z., & Chang, H.-C. (2005). AC electrospray biomaterials synthesis. *Biomaterials, 26*(31), 6122–6128.
Yeo, L. Y., Lastochkin, D., Wang, S.-C., & Chang, H.-C. (2004). A new ac electrospray mechanism by Maxwell-Wagner polarization and capillary resonance. *Physical Review Letters, 92*(13), 133902.
Yuill, E., Shi, W., Poehlman, J., & Baker, L. (2015). Scanning electrospray microscopy with nanopipets. *Analytical Chemistry, 87*(22), 11182–11186.
Zeleny, J. (1914). The electrical discharge from liquid points, and a hydrostatic method of measuring the electric intensity at their surfaces. *Physical Review, 3*, 69–91.
Zeleny, J. (1917). Instability of electrified liquid surfaces. *Physical Review, 10*, 1–6.
Zhao, Y., & Jiang, L. (2009). Hollow micro/nanomaterials with multilevel interior structures. *Advanced Materials, 21*(36), 3621–3638.